

**FOUR-POINT BENDING TENSILE STRENGTH AND
DEFORMATION OF ROCK SALT UNDER CYCLIC
LOADING**

Thanapon Kaewpuang



**A Thesis Submitted in Partial Fulfillment of the Requirements for the
Degree of Master of Engineering in Civil, Transportation
and Geo-resources Engineering
Suranaree University of Technology
Academic Year 2018**

กำลังดึงแบบแรงดัดที่สุดและการเปลี่ยนแปลงรูปร่างของเกลื่อหินภายใต้แรง
แบบวัฏจักร



วิทยานิพนธ์นี้เป็นส่วนหนึ่งของการศึกษาตามหลักสูตรปริญญาวิศวกรรมศาสตรมหาบัณฑิต
สาขาวิชาวิศวกรรมโยธา ขนส่ง และทรัพยากรธรณี
มหาวิทยาลัยเทคโนโลยีสุรนารี
ปีการศึกษา 2561

**FOUR-POINT BENDING TENSILE STRENGTH AND
DEFORMATION OF ROCK SALT UNDER CYCLIC LOADING**

Suranaree University of Technology has approved this thesis submitted in partial fulfillment of the requirements for a Master's Degree.

Thesis Examining Committee



(Asst. Prof. Dr. Akkhapun Wannakomol)

Chairperson



(Asst. Prof. Dr. Decho Phueakphum)

Member (Thesis Advisor)



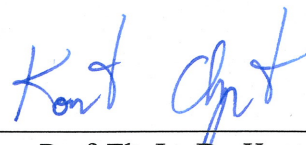
(Assoc. Prof. Dr. Pornkasem Jongpradist)

Member



(Prof. Dr. Santi Maensiri)

Vice Rector for Academic Affairs
and Internationalization



(Assoc. Prof. Ft. Lt. Dr. Kontorn Chamniprasart)

Dean of Institute of Engineering

นายชนพล แก้วพวง : กำลังดึงแบบแรงตัดสี่จุดและการเปลี่ยนแปลงรูปร่างของเกลือหิน
ภายใต้แรงแบบวัฏจักร (FOUR-POINT BENDING TENSILE STRENGTH AND
DEFORMATION OF ROCK SALT UNDER CYCLIC LOADING) อาจารย์ที่ปรึกษา :
ผู้ช่วยศาสตราจารย์ ดร. เดโซ เพ็ญภูมิ, 78 หน้า.

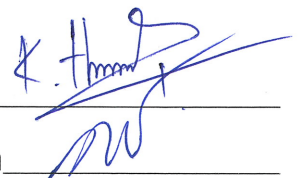
วัตถุประสงค์ของการศึกษานี้คือ เพื่อประเมินผลกระทบของการให้แรงแบบวัฏจักรต่อกำลัง
รับแรงดึงของเกลือหิน โดยการทดสอบแบบแรงตัดสี่จุด ตัวอย่างเกลือหินถูกจัดเตรียมให้มีรูปร่างทรง
สี่เหลี่ยมขนาด 50×50×200 ลูกบาศก์มิลลิเมตร สำหรับทดสอบโดยการให้แรงแบบวัฏจักรภายใต้
สถานะการให้ความเค้นกดกับความเค้นดึงด้วยความความถี่ 0.1 และ 1.0 มิลลิเฮิร์ตซ์ ค่าความเค้น
และความเครียดในแบบดึงและแบบกดที่เกิดขึ้นบนผิวด้านบนและด้านล่างของตัวอย่าง ซึ่งได้ถูก
ตรวจวัดจนกระทั่งตัวอย่างเกิดการวิบัติ ผลการทดสอบพบว่าจำนวนรอบในการให้แรงจนถึงจุด
วิบัติจะเพิ่มขึ้นตามการลดลงของช่วงความกว้างและความถี่ของความเค้น ความเครียดสะสมที่จุด
วิบัติจะเพิ่มขึ้นอย่างเห็นได้ชัดเมื่อช่วงความกว้างและความถี่ของความเค้นลดลง อีกทั้งโมดูลัสความ
ยืดหยุ่นแบบดึงยังมีค่าลดลงตามการเพิ่มขึ้นของช่วงความกว้างและความถี่ของความเค้นด้วยเช่นกัน
ตัวอย่างหลังการวิบัติที่สังเกตได้ แสดงให้เห็นถึงลักษณะการแตกสองลักษณะคือ การแตกระหว่าง
ผลึกและการแตกตามแนวของผลึก ซึ่งรอยแตกระหว่างผลึกบนผิวหน้าของตัวอย่างทดสอบที่
ทดสอบภายใต้ความถี่ต่ำนั้นพบได้มากกว่าที่ทดสอบภายใต้ความถี่สูง รอยแตกที่เกิดขึ้นจากการ
ทดสอบภายใต้ความถี่สูงจะราบเรียบกว่าที่เกิดขึ้นจากการทดสอบภายใต้ความถี่ต่ำ พลังงานที่เกิดขึ้น
ที่จุดวิบัติภายใต้ความเค้นดึงพบว่าการทดสอบที่ความถี่ของความเค้นต่ำจะมีค่าน้อยกว่าพลังงานที่
เกิดจากการทดสอบภายใต้ความถี่ของความเค้นสูง

สาขาวิชาเทคโนโลยีธรณี

ปีการศึกษา 2561

ลายมือชื่อนักศึกษา _____

ลายมือชื่ออาจารย์ที่ปรึกษา _____



THANAPON KAEWPUANG : FOUR-POINT BENDING STRENGTH
AND DEFORMATION OF ROCK SALT UNDER CYCLIC LOADING.

THESIS ADVISOR : ASST. PROF. DECHO PHUEAKPHUM, Ph.D., 78 PP.

BENDING TEST/CYCLIC LOADING/FATIGUE/ROCK SALT/TENSION

The objective of this study is to access the effects of cyclic loading on the tensile strength of rock salt using four-point bending test. The rock salt specimens are prepared as prismatic blocks with nominal dimensions of $50 \times 50 \times 200 \text{ mm}^3$ for cyclic loading test under compression-to-tension with loading frequencies of 0.1 and 1.0 mHz. The stresses and strains in tension and compression which induce on the upper and lower surfaces of specimens are measured until failure occur. The results indicate that the number of loading cycles to failure increases with the applied stress amplitudes and frequencies decreasing. The accumulated strains at failure clearly increase as the stress amplitudes and frequencies decreasing. The tensile elastic modulus also decreases with stress amplitudes and frequencies increasing. Post-failure observations show two fracturing modes: inter-granular and cleavage fracturing. Inter-granular fracturing is found in specimens tested under low loading frequency more than under high loading frequency. Fractures induced under high frequency appear to be smoother than those under low frequency. The energy required to induce tensile failure for the low stress frequency is lower than those obtained from the high stress frequency.

School of Geotechnology

Academic Year 2018

Student's Signature _____

Advisor's Signature _____



ACKNOWLEDGMENTS

I wish to acknowledge the funding support from Suranaree University of Technology (SUT).

I would like to express my sincere thanks to Prof. Dr. Kittitep Fuenkajorn for his valuable guidance and efficient supervision. I appreciate his strong support, encouragement, suggestions and comments during the research period. I also would like to express my gratitude to Asst. Prof. Dr. Decho Phueakphum and Dr. Thanittha Thongprapha for their constructive advice, valuable suggestions and comments on my research works as thesis committee members. Grateful thanks are given to all staffs of Geomechanics Research Unit, Institute of Engineering who supported my work.

Finally, I would like to thank beloved parents for their love, support and encouragement.

Thanapon Kaewpuang

มหาวิทยาลัยเทคโนโลยีสุรนารี

TABLE OF CONTENTS

	Page
ABSTRACT (THAI)	I
ABSTRACT (ENGLISH)	II
ACKNOWLEDGEMENTS	III
TABLE OF CONTENTS	IV
LIST OF TABLES	VII
LIST OF FIGURES	VIII
SYMBOLS AND ABBREVIATIONS	XII
CHAPTER	
I INTRODUCTION	1
1.1 Background and rationale	1
1.2 Research objectives	2
1.3 Scope and limitations	3
1.4 Research methodology	3
1.4.1 Literature review	4
1.4.2 Sample preparation	5
1.4.3 Laboratory testing	5
1.4.4 Mathematical relations	7
1.4.5 Applications	7

TABLE OF CONTENTS (Continued)

	Page
1.4.6 Discussions and Conclusions.....	7
1.4.7 Thesis writing.....	8
1.5 Thesis contents.....	8
II LITERATURE REVIEW	9
2.1 Introduction.....	9
2.2 Time-dependency of salt.....	8
2.3 Cyclic loading test.....	12
2.3.1 Cyclic loading test on rock salt.....	13
2.3.2 Cyclic loading test in tension.....	19
2.4 Fatigue of salt in tension.....	21
2.5 Bending test.....	22
2.5.1 Three-point bending test.....	22
2.5.2 Four-point bending test.....	24
2.6 Tensile strength of salt.....	28
2.7 Loading rate effects.....	30
2.8 Storage in rock salt.....	33
III SAMPLE PREPARATION	35
3.1 Introduction.....	35
3.2 Sample preparation.....	35
3.3 Strain gage installation.....	37

TABLE OF CONTENTS (Continued)

	Page
IV LABORATORY TESTING METHOD	39
4.1 Introduction.....	39
4.2 Test method.....	39
V TESTING RESULTS	44
5.1 Introduction.....	44
5.2 Four point bending with cyclic loading test results	44
VI ANALYSIS OF TEST RESULTS	
6.1 Introduction.....	55
6.2 Analysis.....	55
VII STRAIN ENERGY DENSITY CRITERION	69
7.1 Introduction.....	69
7.2 Strain energy density criterion.....	69
VIII DISCUSSIONS, CONCLUSIONS AND RECOMMENDATIONS FOR FUTURE STUDIES	74
8.1 Discussions	74
8.2 Conclusions.....	76
8.3 Recommendations for future studies	77
REFERENCES	79
APPENDIX A PUBLICATION	87
BIOGRAPHY	91

LIST OF TABLES

Table	Page
3.1 Salt specimens prepared for cyclic loading tests.	38
5.1 Cyclic loading tests results.....	46
5.2 The results are constant stresses under cyclic loading test.	52
6.1 Cyclic loading tests results of TC loading tests (Plangklang et al., 2017) and CTC loading tests	57
6.2 Burger parameters under TC (Plangklang et al., 2017) and CTC tests.....	67
7.1 Strain energy densities of cyclic loading	72

LIST OF FIGURES

Figure	Page
1.1 Cycles of retrieval and injection of storage cavern in rock salt.....	2
1.2 Cyclic loading paths for TC loading (a) and CTC loading (b) used in this Study.....	3
1.3 Research methodology.....	4
1.4 Test arrangement for four-point bending test ASTM D6272-10, and loading configurations for CTC test.....	6
2.1 Typical deformation as a function of time of creep materials (Jeremic, 1994).	10
2.2 Typical stress-strain curve for rock materials (Kumar, 1968; Liang et al., 2010).....	11
2.3 Examples of tensile stresses (σ_x) as a function of tensile strain (ϵ_x) measured for TC loading at $f = 10$ mHz (a) and at $f = 1$ mHz (b) by Plangklang (2017).....	18
2.4 Tensile stress-strain curves for various loading rates by Plangklang (2017).....	19
2.5 Load-deformation curves of Brazilian split fatigue tests of constant average load (Wang et al., 2016).	20
2.6 Load-deformation curves of Brazilian split fatigue tests of variation average load (Wang et al., 2016).....	21

LIST OF FIGURES (Continued)

Figure	Page
2.7	Schematic of a suitable apparatus for flexure test by center-point loading method (ASTM (C293-02))..... 23
2.8	Loading Diagram (ASTM (D6272-10))..... 25
2.9	Elastic beam with (a) fixed ends and (b) simple (pin) supports. 27
2.10	Beam tensile test results showing that the UTS is an exponential function of the beam length / height ratio (Forster, 1967 and Sen, 1961) 29
2.11	Tensile stress-strain curves for various loading rates (Chobsranoi and Fuenkajorn, 2016) 32
3.1	Example of prismatic salt specimens with nominal dimensions of $50 \times 50 \times 200 \text{ mm}^3$ 36
3.2	Some salt specimens prepared for four point bending test with $L/D = 4$ 36
3.3	Example of prismatic salt specimen with strain gage position salt specimens prepared for four point bending test. 37
4.1	Test arrangement for four-point bending test (ASTM (D6272-10) under compression-to-tension loading..... 40
4.2	Four point bending test apparatus 41
4.3	Stress distribution at mid-section of specimen. 41

LIST OF FIGURES (Continued)

Figure	Page
5.1	Compressive and tensile stresses (σ_x) as a function of compressive and tensile strains (ϵ_x) measured for cyclic loading at $f = 1$ mHz (a) and at $f = 0.1$ mHz (b).45
5.2	Fatigue tensile stress (σ_T) as a function of loading cycles.....47
5.3	Normalized tensile elastic modulus (E/E_0) plotted as a function of number of loading cycles (N) up to failure for cyclic loading tests.....49
5.4	Fracture surfaces and their laser-scanning profiles for high loading frequencies (a), and for low loading frequencies (b). Cleavage fracturing highlighted in dark area.....50
5.5	Some post-test specimens of Maha Sarakham salt obtained from four point bending testing under cyclic loading test.....51
5.6	Compressive strain (ϵ_c) as a function of time for cyclic loading tests at $f = 0.1$ mHz53
5.7	Compressive strain (ϵ_c) as a function of time for cyclic loading tests at $f = 1.0$ mHz.53
5.8	Tensile strain (ϵ_t) as a function of time for cyclic loading tests at $f = 0.1$ mHz.....54
5.9	Tensile strain (ϵ_t) as a function of time for cyclic loading tests at $f = 1.0$ mHz.....54

LIST OF FIGURES (Continued)

Figure	Page
6.1	Cyclic loading paths for TC loading (a) (Plangklang et al., 2017) and CTC loading (b) used in this study56
6.2	Fatigue tensile stress (σ_T) as a function of number of loading cycles at failure (N) for TC (Plangklang et al., 2017) and CTC tests..... 58
6.3	Fatigue tensile strains as a function of number of loading cycles (N) for TC (Plangklang et al., 2017) and CTC tests.....59
6.4	Normalized tensile elastic modulus (E/E_0) plotted as a function of number of loading cycles (N) up to failure for TC loading tests (a) by Plangklang et al. (2017) and CTC loading tests (b)..... 60
6.5	Fracture surfaces and their laser-scanning profiles for TC test (a) (Plangklang et al., 2017), and for CTC test (b)..... 62
6.6	Tensile strains (ϵ_x) as a function of time for TC loading tests (Plangklang et al., 2017). 65
6.7	Tensile strains (ϵ_x) as a function of time for CTC loading tests. 66
6.8	Visco-plastic coefficients (η_1) as a function of tensile stress for TC (Plangklang et al., 2017) and CTC tests 68
7.1	Distortional strain energy (W_d) as a function of mean strain energy (W_m) at failure.....73

SYMBOLS AND ABBREVIATIONS

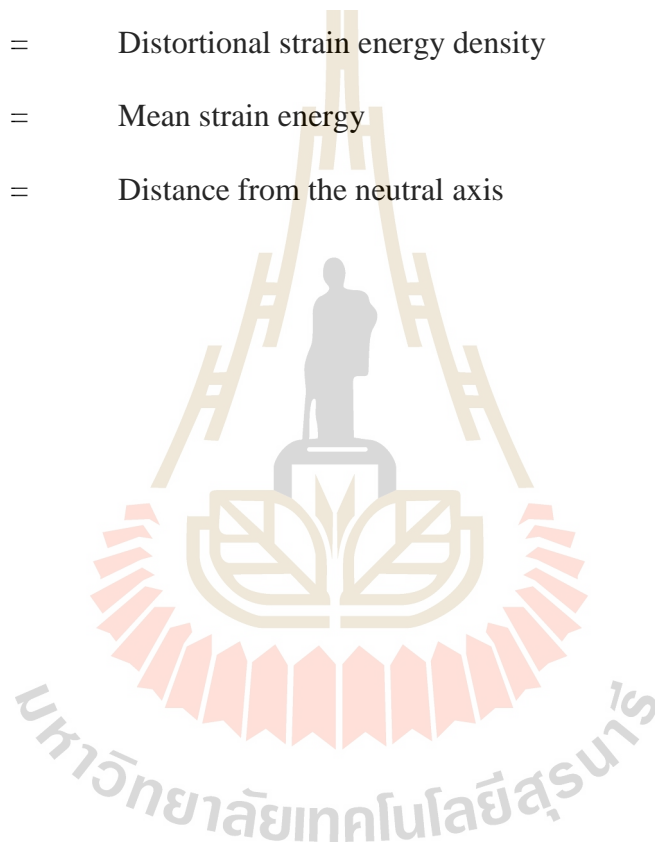
η	=	Empirical constant
η_1	=	Viscosity coefficient in steady-state phase
η_2	=	Viscosity coefficient in transient phase
β	=	Empirical constants
α	=	Empirical constants
f	=	frequency
ν	=	Poisson's ratio
σ	=	Stress
σ_c	=	Maximum compressive stress
σ_T	=	Fatigue tensile stress
σ_t	=	Maximum tensile stress
$\sigma_x, \sigma_y, \sigma_z$	=	Principal stresses
ϵ_c	=	Maximum compressive strains
ϵ_e	=	Instantaneous elastic strain
ϵ_p	=	Permanent strain
ϵ_t	=	Maximum tensile strains
$\epsilon_x, \epsilon_y, \epsilon_z$	=	Principal strain
$\partial\sigma/\partial t$	=	Constant stress rate

SYMBOLS AND ABBREVIATIONS (Continued)

b	=	Nominal width
CAES	=	Compressed air energy storage
CTC	=	Compression-to-tension cyclic loading
d	=	Nominal thickness
D	=	Specimen diameter
E	=	Elastic modulus
E_0	=	Normalized elastic
E_1	=	Tensile spring constant
E_2	=	Spring constant in visco-elastic phase
E_B	=	Modulus of elasticity in bending
e	=	Mean strain
e_x, e_y, e_z	=	Strain deviations in major, intermediate and minor axes
F	=	Compressive force acting
I	=	Moment of inertia
L	=	Nominal length
M	=	Bedding moment
N	=	Number of loading cycles
NaCl	=	Sodium chloride
P	=	Applied load
r	=	Loading rate
R	=	Modulus of rupture

SYMBOLS AND ABBREVIATIONS (Continued)

s	=	Mean stress
s_x, s_y, s_z	=	Stress deviations in major, intermediate and minor axes
t	=	Time
TC	=	Tension cyclic loading
W_d	=	Distortional strain energy density
W_m	=	Mean strain energy
y	=	Distance from the neutral axis



CHAPTER I

INTRODUCTION

1.1 Background and rationale

Rock salt around storage caverns will subject to cycles of loading due to the fluctuation of cavern pressures during product injection and retrieval periods, as shown in Figure 1.1. The cavern roof, in particular, may subject to cycles of compression and tension, depending on the maximum and minimum storage pressures as they are the main factors controlling the loading magnitude. The fatigue characteristics has significant effects on storage safety because of the pressure changes that occur during gas injection and production. The loading cycles can reduce the salt strength, depending on the loading amplitudes and the maximum applied loads in each cycle (Haimson, 1978; Wang et al., 2016). Much of the research works have been concentrated on the material fatigue due to the monotonic loading and unloading: tensile cyclic loading (TC), as shown in Figure 1.2(a). Under actual in-situ conditions however the loading cycles may involve both tension and compression. Such forward and reverse loading paths are likely to occur at the salt roof of storage cavern

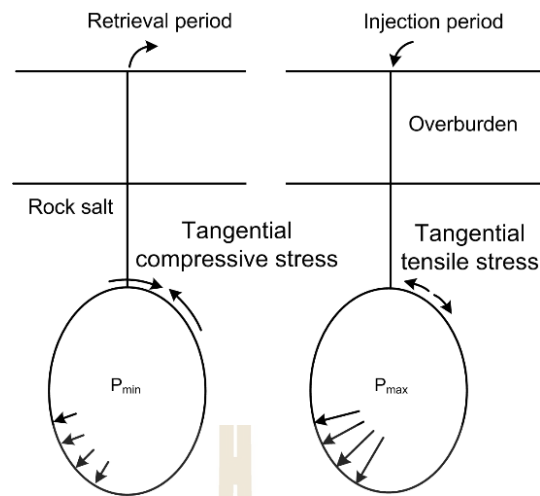


Figure 1.1 Cycles of retrieval and injection of storage cavern in rock salt.

1.2 Research objectives

The objective of this study is to experimentally assess the effects of loading cycles and paths on tensile strength of rock salt. The tensile strengths are obtained by performing four-point bending test on prismatic beams ($50 \times 50 \times 200 \text{ mm}^3$) of rock salt specimens. The loading path is based on compression-to-tension cyclic loading (CTC), as shown in Figure 1.2(b) with loading frequencies of 0.1 and 1.0 mHz. The induced tensile strains are measured with strain gage until failure occurs. Strain energy density principle is applied to describe the effect of loading cycles and paths on the fatigue tensile strengths of the rock salt specimens. The findings can be used to determine salt maximum and minimum cavern pressures for long term stability.

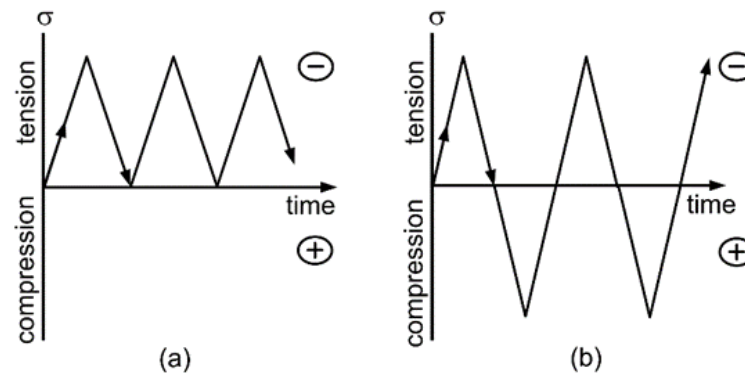


Figure 1.2 Cyclic loading paths for TC loading (a) and CTC loading (b) used in this Study.

1.3 Scope and limitations

The scope and limitations of the research include as follows.

1. All specimens are conducted on rock specimens obtained from Lower Member of the Maha- Sarakham formation.
2. The nominal dimensions of prismatic blocks are $50 \times 50 \times 200 \text{ mm}^3$.
3. The maximum tensile stresses and the loading frequencies range from 0.40 to 1.40 MPa and 0.1 to 1 mHz, respectively.
4. The testing procedure follow the relevant standard practices (ASTM D6272-10).
5. The research findings are published in conference paper and journal.

1.4 Research methodology

The research methodology shown in Figure 1.3 comprises 7 steps; including literature review, sample preparation, four point bending cyclic tests, mathematical relations, application, discussions and conclusions and thesis writing.

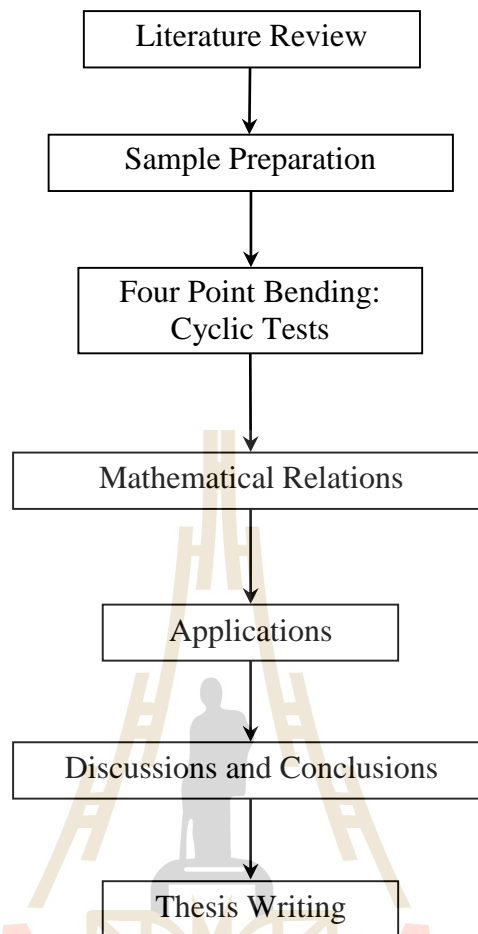


Figure 1.3 Research methodology.

1.4.1 Literature review

Literature review is carried out to study the previous researches on time-dependency of salt in tension, cyclic loading test, cyclic loading of salt in tension, fatigue of salt in tension, tensile strength, compressed-air energy storage, computer simulations. The sources of information are from text books, journals, technical reports and conference papers. A summary of the literature review is given in chapter 2.

1.4.2 Sample preparation

Rock samples used here have been obtained from underground openings of ASEAN Potash Chaiyaphum Public Company Limited (APOT). They belong to the Lower Salt member of the Maha Sarakham formation. Sample preparation are carried out in the laboratory at Suranaree University of Technology. The specimens are prepared to obtain prismatic blocks with nominal dimensions of $50 \times 50 \times 200 \text{ mm}^3$.

1.4.3 Laboratory testing

Laboratory tests include four-point bending tests following ASTM D6272-10. Figure 1.4 shows the loading directions for both compression-tension cyclic loading (CTC) testing. The positions of the loading for the upper and lower bearing plates. A data logger (TC-32K) connected with the switching box (Type B-2760) is used to monitor the induced compressive and tensile strains.

The four point bending with CTC tests uses two sets of the loading platens to obtain the alternate compression-to-tension loading. The specimens used for the CTC loading are subjected to the loading frequencies of 0.1 and 1 mHz.

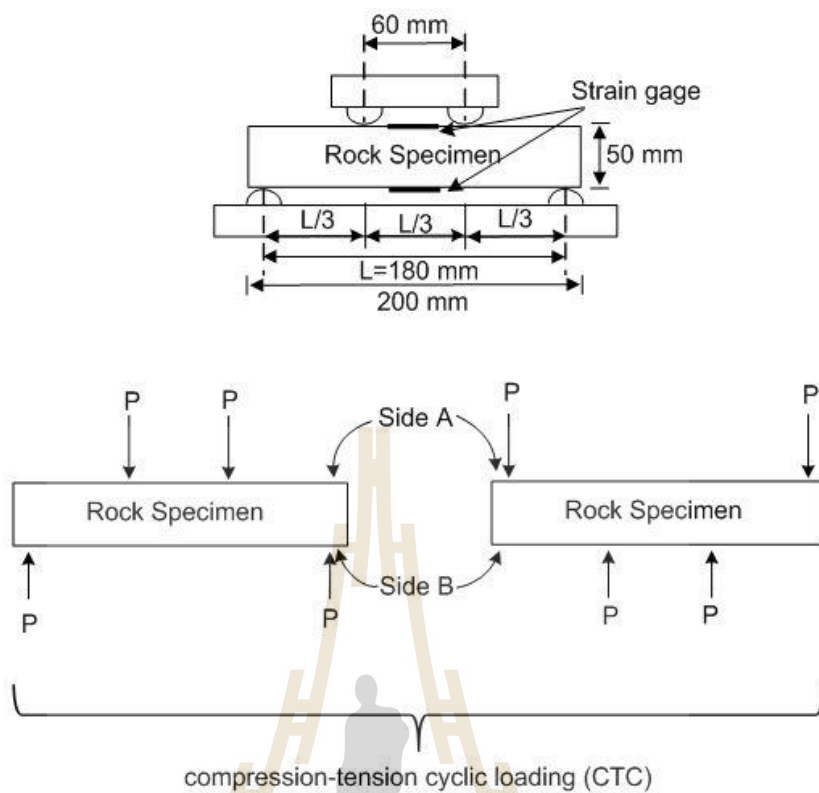


Figure 1.4 Test arrangement for four-point bending test ASTM D6272-10, and loading configurations for CTC test.

1.4.4 Mathematical relations

The results are used to describe the deformability of rock salt specimens with time dependency under mechanical cyclic loads. Regression analyses on the strain-time curves based using the SPSS statistical software are performed to determine these parameters for each rock salt specimen. The strain energy density principle is applied to describe the salt strengths and deformability under different frequencies and amplitudes of cyclic loading tests. The relations are used to calculate the stability of rock salt specimens in the laboratory.

1.4.5 Applications

The laboratory testing can be used to predict and design of salt caverns for compressed-air energy. Strain energy density principle is applied to describe the effect of loading cycles and paths on the fatigue tensile strengths of the rock salt specimens. The calculated roof stresses combining with the strain energy criterion are used to determine the critical tensile strains that the roof can sustain before failure occurs. By substituting the critical strain into the strain-time curves the standup time for the roof under static and cyclic loading can be predicted.

1.4.6 Discussions and Conclusions

Discussions are made on the impacts of the mechanical cyclic loads on the storage stability. All research activities, methods, and results are documented and compiled in the thesis. The research or findings are published in the conference proceedings or journals.

1.4.7 Thesis writing

All research activities, methods, and results are documented and compiled in the thesis.

1.5 Thesis contents

This research thesis is divided into eight chapters. The first chapter introduces the thesis by briefly describing the background of problems and significance of the study. The research objectives, methodology, scope and limitations are identified. The second chapter presents results of the literature review about time-dependency of salt, fatigue of salt in tension, bending test, tensile strength of salt, loading rate effects, cyclic loading of salt in tension and roof stability and design. The chapter three describes sample preparation. The laboratory testing are described in chapter four and testing results are described in chapter five. The testing result and analysis of test result explicated are in chapter five and six respectively. Chapter seven present the method and results of Strain energy density principle analysis on the wall of salt caverns and chapter eight present discussions, conclusions and recommendation for future studies.

CHAPTER II

LITERATURE REVIEW

2.1 Introduction

The topic reviewed here include time-dependency of salt, cyclic loading test, cyclic loading test in tension, fatigue of salt in tension, bending test, tensile strength of salt, loading rate effects and storage in rock salt.

2.2 Time-dependency of salt

The time-dependent deformation (or creep) is the process at which the rock can continue deformation without changing stress (Fuenkajorn and Daemen, 1988; Dusseault and Fordham, 1993; Jeremic, 1994; Knowles et al., 1998). The creep strain seldom can be recovery fully when loads are removed, thus it is largely plastic deformation. Creep deformation occurs in three different phases, as shown in Figure 2.1, which relatively represents a model of salt properties undergoing creep deformation due to the sustained constant load. Upon application of a constant force on the rock salt, an instantaneous elastic strain (ϵ_e) is induced. The elastic strain is followed by a primary or transient strain, shown as Region I. Region II, characterized by an almost constant slope in the diagram, corresponds to secondary or steady state creep. Tertiary or accelerating creep leading to rather sudden failure is shown in Region III. Laboratory investigations show that removal of applied load in Region I at point L will cause the strain to fall rapidly to the M level and then asymptotically back to zero at N.

The distance LM is equal to the instantaneous strain ϵ_e . No permanent strain is induced here if the removal of stress takes place in the steady-state phase the permanent strain (ϵ_p) will occur. From the stability point of view, salt structure deformations after constant load removal have only academic significance, since the stresses imposed underground due to mining operations are irreversible. The behavior of the salts with time-dependent deformation under constant load is characterized as a visco-elastic and visco-plastic phenomenon. Under these conditions the strain criteria are superior to the strength criteria for design purposes, because failure of most salt pillars occurs during accelerated or tertiary phase of creep, due to the almost constant applied load.

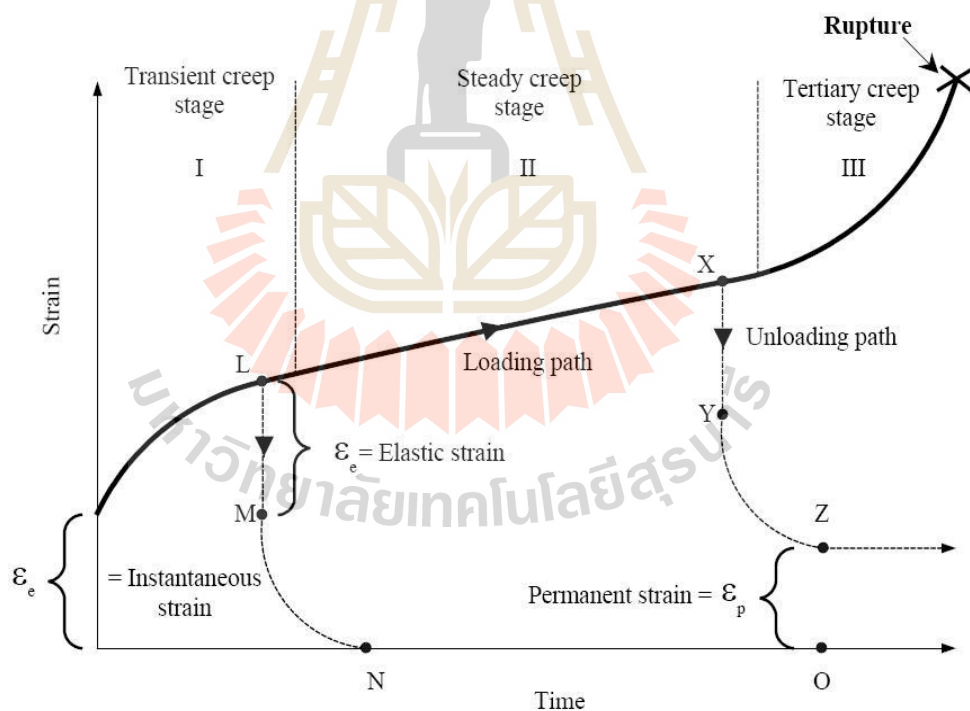


Figure 2.1 Typical deformation as a function of time of creep materials (Jeremic, 1994).

A typical stress versus strain curve for a rock specimen under loading can be divided into four regions as revealed in Figure 2.2. In region I there is a small foot in the curve, and the observed modulus is lower because of the nonelectric strain arising from the closing up of the microcracks and pore. Region II represents the true modulus of the bulk material and the stress versus strain curve here is linear. The stress-strain curve then starts to deviate from linearity in region III indicating the stage of nucleation of microcracks. Here there is a general loosening of the grain boundaries which is not yet obvious in microscopic observations. Only in region IV do microcracks become visible in an optical microscope. The only difference was that regions III and IV of the static stress-strain curve were extended to larger strains. Consequently the fracture strength was increased primarily because of a larger strain-to-fracture (Kumar, 1968; Liang et al., 2010).

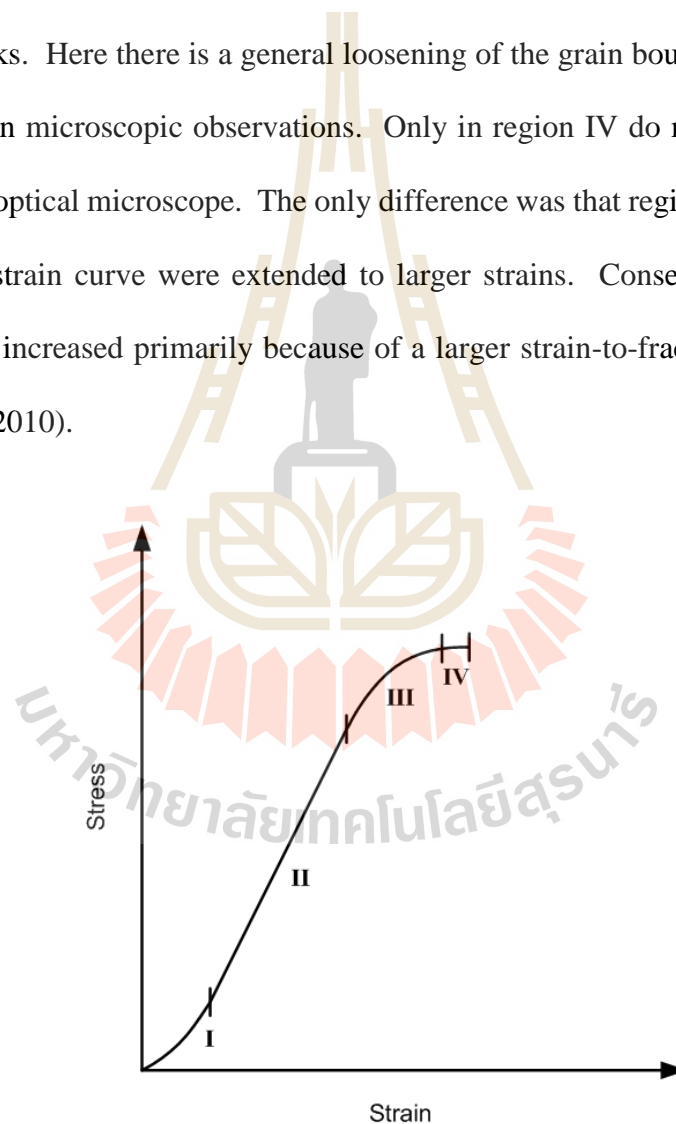


Figure 2.2 Typical stress-strain curve for rock materials (Kumar, 1968; Liang et al., 2010).

2.3 Cyclic loading test

The effect of cyclic loading often results in failure of engineering structures for instance, dam, road and bridge foundations, tunnels or even air storage caverns in bed rocks. The causes could be from earthquake, traffic, blasting and the process of compressed and released air in and out of the cavern to produce electricity, etc. Even civil engineering materials, such as steels, concrete or soil can be also affected by the cyclic loading. However, only the cyclic loading test on rock will be discussed here. The objective of the cyclic loading test in rock salt is to understand the duration of structures under cyclic loading and to apply the results in designing of air controlling systems during CAES operation. A rock salt cavern is subjected to pressure changes. The pressure will be high and low in cyclic manner according to its operation. The duration of the cavern can be referred from the number of pressurized cycles before cracking will take place. This also depends on characteristic of the acting pressure (Passaris, 1982). Most of fatigue test results from cyclic loading show relationship between stress and strain, fatigue stress and number of cycles that cause failure or fatigue life (S-N curve).

From previously studied, the effect of cyclic loading on rock salt under uniaxial and triaxial compression tests has been investigated to determine the fatigue lives of the storage wall in salt mass (Fan et al., 2016, 2017; Song et al., 2013; Yasong et al., 2016). Some researchers have been studied the effect of tensile cyclic loading on the mechanical behavior of several rock types, such as Erarslan and Williams (2012) studied on Brisbane tuff, Voznesenskii et al. (2016) on gypsum, Cardani and Meda (2004) on marble and Wang et al. (2016) on rock salt. The loading cycles can reduce the fatigue strength and elastic modulus, depending on the loading amplitudes (Ren et

al., 2013; Guo et al., 2012), loading frequency (Momeni et al., 2015) and maximum applied loads for each cycle (Song et al., 2013; Wang et al., 2016).

2.3.1 Cyclic loading test on rock salt

Thoms et al. (1980) perform triaxial cyclic loading with low frequency (24 cycles/10 hrs.) by imitating the actual loading condition of the CAES in rock salt cavern. The study was also carried out with an aid of the computer model. The specimen with a diameter of 100 mm and length of 200 mm is subjected to cyclic loading at 34.5 MPa. The temperature is systematically increased and decreased. They found that change of temperature in the cycle would result in creep of the rock salt. The frequency affects the behavior of rock salt under the cyclic loading. The different frequency causes difference in number of cycles that causes failure, even subjected to same loading characteristic. Number of cycles that cause failure in the higher frequency is more than the number of cycles in the lower frequency. The higher stress level (fatigue stress), the number of cycles that causes failure is less than that in the lower stress level.

Passaris (1982) investigates the cyclic loading test on rock salt in order to design compressed air energy storage cavern. The tests are performed at low frequency (0.1 Hz). First, in each cycle, load had been increased up to the designed load and then decreased to zero, or called "full unloading". The maximum loads ranged between 60-80% of uniaxial compressive strength. The tests had been done on 16 specimens. The amounts of loading cycles were limited at 10,000 cycles. For the second series, the applied load increased to the designed load and then decreased partially, called "partial unloading. The applied load is imitated from the up-down pressure in the rock salt cavern. The relationship between the fatigue strength (s) and the fatigue life (number of cycles causing failure-N): $S = 1.91N - 1.91N^{-0.05}$. The rock salt can soften

by cyclic loading and the elastic modulus can decrease as the number of cycles increase. The test reveals that the fatigue stress limit of rock salt is at 60% of the uniaxial compressive strength. The further suggests that during releasing air from the cavern, the pressure in the cavern should be maintained higher than 55% of the rock salt strength.

Gehle and Thoms (1986) study the change in acoustic emission (AE) characteristics causing by cyclic loading in rock salt cavern. They drilled two holes with angle of 45 from horizontal, with a diameter of 57 mm and 6.1 m deep into the base of craven pillar. Another drilled hole with a diameter of 64 mm is drilled at the middle of two holes. The signal interpretation equipment is put into the first two holes, whereas the equipment for applying cyclic load namely hydraulic pressure is placed in the middle hole. The result from the test showed that the AE signal pattern increased as the pressure in the drilled holed increased. This means that cracks have developed. The summary indicates that the AE-method could be used to measure the change in rock salt property which is affected by the cyclic loading and can also indicate that cracks development as the number of loading cycles increases.

Fuenkajorn and Phueakphum (2010) perform cyclic loading tests on the Maha Sarakham salt. Their results indicate that the salt compressive strength decreases with increasing number of loading cycles, which can be best represented by a power equation. The salt elastic modulus decreases slightly during the first few cycles, and tends to remain constant until failure. It seems to be independent of the maximum loads. Axial strain–time curves compiled from loci of the maximum load of each cycle apparently show a time-dependent behavior similar to that of creep tests under static loading. In the steady-state creep phase, the visco-plastic coefficients calculated from

the cyclic loading test are about an order of magnitude lower than those under static loading. The salt visco-plasticity also decreases with increasing loading frequency. Surface subsidence and cavern closure simulated using parameters calibrated from cyclic loading test results are about 40% greater than those from the static loading results. This suggests that application of the property parameters obtained from the conventional static loading creep test to assess the long-term stability of storage caverns in salt with internal pressure fluctuation may not be conservative.

Ma et al. (2013) study the mechanical properties of rock salt under triaxial cyclic loading for design the underground energy storage. The rock sample a set of 11 specimens are obtained from Qianjiang salt deposit located at a depth of 1990–2080 m. underground in Hubei Province. Three samples are prepared for conventional triaxial compression tests, and the remaining eight samples are used for cyclic loading tests. Both conventional triaxial compression and cyclic loading tests were applied at confining pressures of 7 MPa, 14 MPa and 21 MPa at a constant stress-controlled rate of 0.05 MPa/s. Conventional triaxial compression tests were conducted using a GAW-2000 mechanical frame at a constant axial strain rate of $5 \times 10^{-4} \text{ s}^{-1}$. For the cyclic loading tests, the axial load is specified as a sinusoid ally cyclic compressive load, and the loading frequency is set to 0.025 Hz, 0.05 Hz and 0.1 Hz, respectively.

Song et al. (2013) perform cyclic loading tests to determine the fatigue life on rock salt. The testing includes uniaxial and triaxial cyclic loading tests under different upper and lower stresses, speeds of cyclic loading, temperatures, and confining pressures for evaluate the safety levels of storage caverns in rock salt. The rock salt samples are cut into circular cylinders 50 mm diameter 100 mm length collected from depths of 1000 m at sites in the Himalayas. The testing under different

maximum stresses are 95%, 90%, 85%, and 80% of the compression strength and minimum stresses of 20%, 30%, 40%, and 50% of the compression strength, the average fatigue lives are 68, 85, 142, and 374, respectively. The testing under different loading speeds are 0.36 kN/s, 1 kN/s, 3 kN/s, 5 kN/s, 7 kN/s, and 10 kN/s, set to 90% and 20% of the average compressive strength.

For the testing under different temperatures, the salt rock are divided into six groups. In the first three groups were subjected to uniaxial compression at 13°C, 30°C, and 60°C obtained under different temperatures 47 MPa (at 13°C), 43 MPa (at 30°C), and 40 MPa (at 60°C). The other three groups were loaded at 13°C, 30°C, and 60°C with the upper and lower stress levels set at 20% and 90% of the average compressive strength for each temperature 9.4 MPa and 42.3 MPa (at 13°C), 8.6 MPa and 38.7 MPa (at 30°C), 8 MPa and 36 MPa (at 60°C).

For the testing under different confining stresses the rock salt specimens are divided into six groups. In the first three groups are subjected to compression with confining pressures of 0 MPa, 3 MPa, and 5 MPa, and the average compressive strengths were 47 MPa, 75 MPa, and 90 MPa, respectively. The other three groups are subjected to cyclic loading with confining pressures of 0 MPa, 3 MPa, and 5 MPa and upper and lower stresses that were equal to 20% and 90% of the average compressive strength. The lower and upper stresses were 9.4 and 42.3 MPa, 15 and 67.5 MPa, and 18 and 81 MPa for confining pressures of 0 MPa, 3 MPa, and 5 MPa, respectively. The results show the fatigue limit of rock salt equal to 75% of the compressive strength. The results can be useful to determining the pressure limits of gas injection and production of gas storage in salt rock.

Plangklang (2017) perform four-point bending under cyclic loading tests (Figure 2.3). The loading frequencies range from 1 to 10 mHz. The induced maximum tensile stresses range from 1.21 to 3.20 MPa. The results indicate that the permanent strain increase and accumulates from each cycle until the specimen fails. The number of loading cycle increases with decreasing the maximum applied stresses (amplitudes) and loading frequency increased. Relation between the number of cycles (N) and fatigue tensile strength (S) indicate that the effect of loading frequency is relatively small. The strength difference between 1 mHz and 10 mHz is about to 10%. Elastic modulus of rock salt derived from the cyclic loading test results decrease as the number of cycles increase. The elastic moduli obtained from the test are varied from 0.47 GPa to 1.93 GPa.

The effect of and loading rate (Figure 2.4) on the rock tensile strength is assessed under five constant rates from 1×10^{-7} to 1×10^{-3} MPa/s. The results show that the tensile strength increases with increasing loading rates, and tensile strains decreases with increasing loading rates. The tensile elastic modulus is lower than the compressive elastic modulus. The higher deflection occurs under lower loading rate.

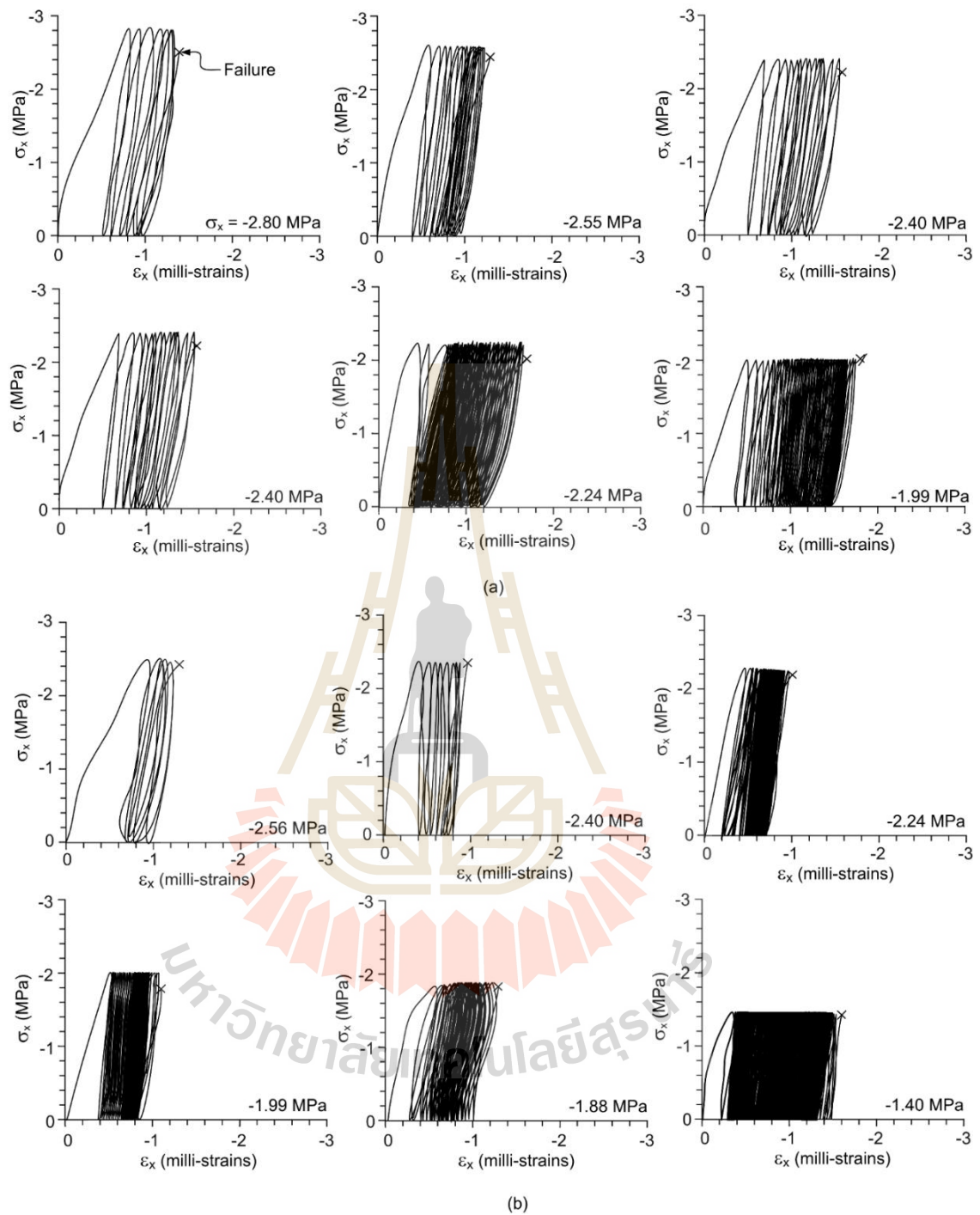


Figure 2.3 Examples of tensile stresses (σ_x) as a function of tensile strain (ϵ_x) measured for TC loading at $f = 10$ mHz (a) and at $f = 1$ mHz (b) by Plangklang (2017).

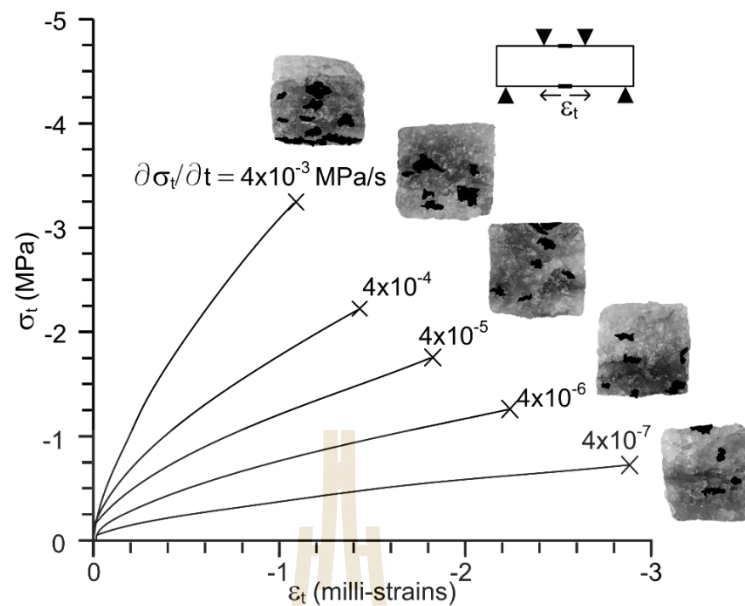


Figure 2.4 Tensile stress-strain curves for various loading rates by Plangklang (2017).

2.3.2 Cyclic loading test in tension

Wang et al. (2016) conducted experiments including Brazillian spiltting test, constant average load splitting fatigue test in which we use constant frequency and constant amplitude sine wave individually, and variable mean load splitting fatigue test. The results of Brazilian split fatigue test can be seen that the load-vertical deformation curve is divided into two parts from Figure 2.5. The first part of the curve is a static loading stage, the load increase at the constant rate of 0.05kN/s till the average load level, and it is a linear relationship between load and deformation. The second part of the curve is a splitting fatigue stage; the cyclic load begins with the average load level at the frequency of 1 Hz. The vertical deformation-load curve of test specimen is shown in Figure 2.6. As can be taken from Figure 2.6, cyclic loading loads 500 times at the first load level and the curve goes through the first stage of the three stages of “sparse-dense-sparse”, resulting in larger deformation.

Improving the average load level and load 500 times, the deformation is less than the first level. It remains at the “dense” stage (second stage); thus, although the average load is slightly larger than previous one, the deformation amount is less than the first stage. The deformation of each stage is gradually increasing with the gradual increase of load level. During the last stage of the load level, the deformation increases rapidly in the course of cyclic loading, and the specimen is suddenly destroyed with the increase of deformation. Conclusion of this paper can be used as part of experiences and reference providing for the gas storage operations in salt caverns.

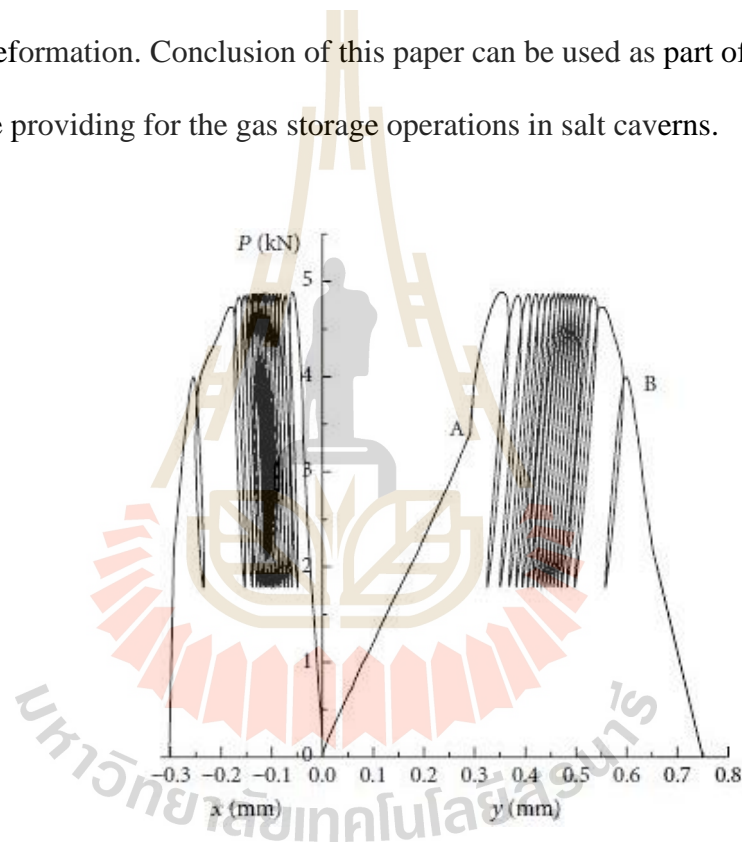


Figure 2.5 Load-deformation curves of Brazilian split fatigue tests of constant average load (Wang et al., 2016).

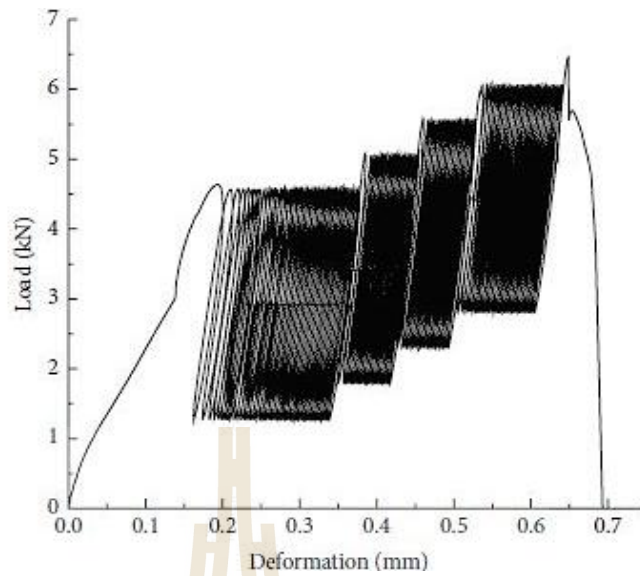


Figure 2.6 Load-deformation curves of Brazilian split fatigue tests of variation average load (Wang et al., 2016).

2.4 Fatigue of salt in tension

The fatigue properties of rock depend on the maximum compressive and tensile stresses generated during cyclic loading, the load amplitude, and the loading frequency (Thirumalai and Demou, 1974; Xiao et al., 2010).

Voznesenskii et al. (2017) experiments with cyclic fatigue loading samples of rock salt (halite) showed a non-monotonic change in strength, depending on the number of load cycles. The minimum strength is observed at 20 cycles for cyclic loadings up to 40%, and 60% from damage tension at 15 cycles until 80% loading. The two most likely mechanisms are dilation, causing strength decrease; and consolidation, due to the cohesion of halite grains under cyclic deformation, causing a strength increase. Their combination reduces the strength of the initial area of the deformation and its subsequent increase after reaching a minimum. These changes

are consistent with changes in the strength storage modulus and volume deformation, depending on the number of loadings. The dependencies between the strength and quality factor will allow the strength of the objects under study to be assessed by non-destructive testing methods while leaving them intact.

2.5 Bending test

2.5.1 Three-point bending test

The American Society for Testing and Materials (ASTM (C293-02)) specifies the methods and sample preparation for the three-point bending test. All forces are applied perpendicular to the face of the specimen continuously without eccentricity. A diagram of an apparatus that accomplishes this purpose is shown in Figure 2.7. The load is applied at a constant rate to the breaking point. The maximum stress on the tension face increases under loading rate between 0.9 and 1.2 MPa/min (125 and 175 psi/min). The loading rate is calculated using the following equation:

$$r = 2Sbd^2 / 3L \quad (2.1)$$

where r is loading rate, N/min (lb/min), S is rate of increase in the maximum stress on the tension face, MPa/min (psi/min), b is average width of the specimen as oriented for testing, mm (in), d is average depth of the specimen as oriented for testing, mm (in.) and L is span length, mm (in).

The modulus of rupture is calculated as follows:

$$R = 3PL / 2bd^2 \quad (2.2)$$

where R is modulus of rupture, MPa (psi), P is maximum applied load indicated by the testing machine, N (lbf), L is span length, mm (in.), b is average width of specimen at the fracture, mm (in.) and d is average depth of specimen at the fracture, mm (in.). A bar of rectangular cross section rests on two supports and is loaded at two points or two loading noses. The distance between the loading noses (the load span) is either one third or one half of the support span.

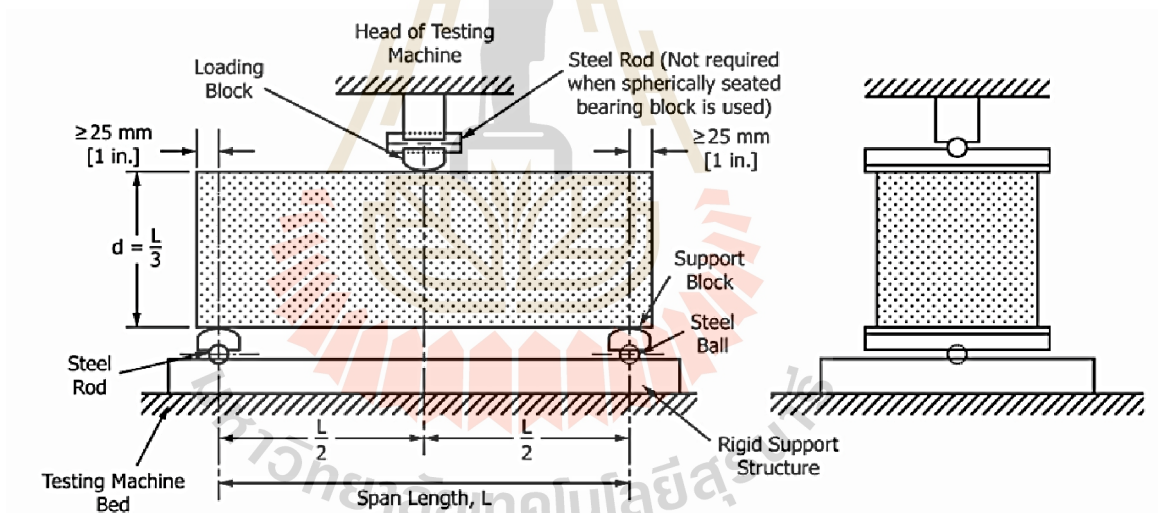


Figure 2.7 Schematic of a suitable apparatus for flexure test by center-point loading method (ASTM (C293-02)).

2.5.2 Four-point bending test

Specifications for standard test method for four-point bending test by American Society for Testing and Materials ASTM (D6272-10). The test method is a bar of rectangular cross section rests on two supports and is loaded at two points or two loading noses, each an equal distance from the adjacent support point. The distance between the loading noses (the load span) is either one third or one half of the support span shown in Figure 2.8.

When a beam is loaded in flexure at two central points and supported at two outer points, the maximum stress in the outer fibers occurs between the two central loading points that define the load span. This stress may be calculated for any point on the load deflection curve for relatively small deflections by the following equation for a load span of one third of the support span:

$$S = PL / bd^2 \quad (2.3)$$

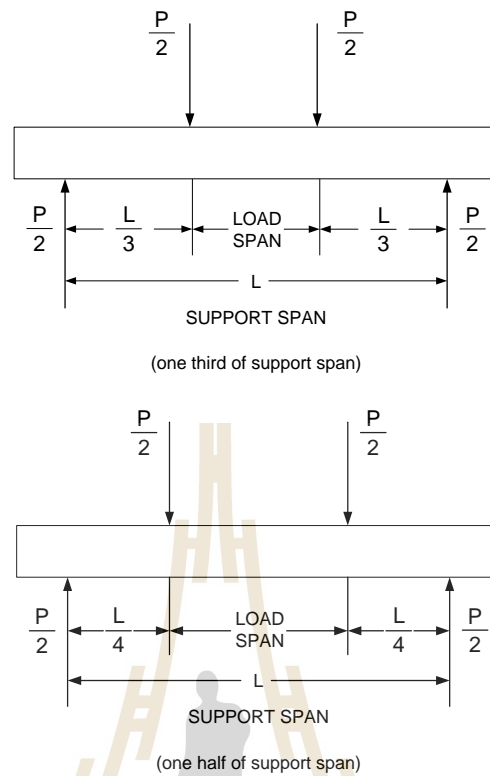


Figure 2.8 Loading Diagram (ASTM (D6272-10)).

For a load span of one half of the support span:

$$S = 3PL / 4bd^2 \quad (2.4)$$

where S is stress in the outer fiber throughout the load span, P is load at a given point on the load-deflection curve, L is support span, b is width of beam and d is depth of beam.

The tangent modulus of elasticity is the ratio, within the elastic limit, of stress to corresponding strain and shall be expressed in megapascals (pounds per square inch). It is calculated by drawing a tangent to the steepest initial straight-line portion of the load-deflection curve and using equation (2.5) for a load span of one third the

support span and equation (2.6) for a load span of one half of the support span, as follows:

$$E_B = 0.21L^3m / bd^3 \quad (2.5)$$

$$E_B = 0.17L^3m / bd^3 \quad (2.6)$$

where E_B is modulus of elasticity in bending, L is support span, B is width of beam tested, D is depth of beam tested and m is slope of the tangent to the initial straight-line.

Obert and Duvall (1967) propose the solution for the maximum stress values at the abutments for compression (bottom of beam) or tension (top of beam) (σ_{\max}) as well as the maximum beam deflection (δ) can be easily calculated using closed form beam equations, as follows:

$$\sigma_{\max} = \gamma S^2 / 2T \quad (2.7)$$

$$\delta = \gamma S^4 / 32ET^2 \quad (2.8)$$

where E is the Young's modulus of the rock, γ is the specific weight and T is thickness.

The maximum stress at the midspan is one half of the maximum stress at the abutments. Therefore, for such a beam with fixed ends and distributed loading, yield is assumed when the maximum tensile stress in the upper part of the beam at the abutments exceeds the tensile strength of the rock. Vertical tensile fractures form at the abutments and the beam becomes simply supported (assuming no slip at the

abutments) as shown in Figure 2.7(b) with a maximum tensile stress at the mid span given by

$$\sigma_{\max} = 2\gamma S^2 / 3T \quad (2.9)$$

This stress is now higher than the previous abutment stress, and therefore higher than the rock tensile strength. This leads to subsequent fracturing centered about the midspan as shown by Stimpson and Ahmed (1992). Snyder (1983) considers a laminated rock beam an excavation with a horizontal span by the normal thickness of the single layer under analysis. An elastic beam with no joints and with constant cross section a distribution of compression and tension symmetrical about the horizontal centreline of the beam is found across all plane sections within the beam as shown in Figure 2.9(a).

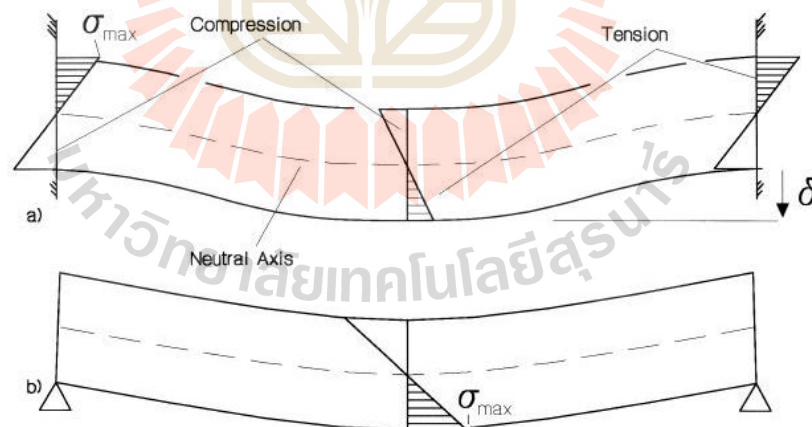


Figure 2.9 Elastic beam with (a) fixed ends and (b) simple (pin) supports. (Snyder, 1983).

Yokoyama (1988) derives a useful formulation for the stress-strain relation in a four-point bending test. His analysis utilizes the experimental measurements of the axial load, P , the strains at the top and bottom of the beam, and the geometry of the device and the beam. The derivations of Yokoyama (1988) lead to the following values of σ_t and σ_c , the maximum tensile stress and the maximum compressive stress along the beam (fiber stresses)

$$\sigma_t = [dM(\varepsilon_t + \varepsilon_c) + 2M(d\varepsilon_t + d\varepsilon_c)] / (bh^2d\varepsilon_t) \quad (2.10)$$

$$\sigma_c = [dM(\varepsilon_t + \varepsilon_c) + 2M(d\varepsilon_t + d\varepsilon_c)] / (bh^2d\varepsilon_c) \quad (2.11)$$

where $M = 0.5P(L_t - L_c)$ is the bending moment of the beam (L_t and L_c are the spacing of pairs of the loading point for the tensile side and for the compressive side, respectively); ε_t and ε_c are the tensile and compressive strain measured at the top and bottom of the deformed beam, respectively (fiber strains); b is the beam width; h is the beam height; dM , $d\varepsilon_t$ and $d\varepsilon_c$ are the increments of the moment and the strain during the experiment (the differentials between two consecutive steps in the experiment).

2.6 Tensile strength of salt

Beam tests were undertaken by Forster (1967) and Sen (1961) on cylindrical and prismatic rock salt specimens, using either a three-point or four-point loading device, with aim of determining the flexural strength, and hence the tensile strength of the outer fiber of the material. The results of beam bending (three point, four point and uniformly loaded) are in general higher than those from the Brazilian disc tests. Figure 2.10 also confirms that the tensile strength is an exponential function of the

length/height ratio of the salt beam. The beam test results showed a significant variation depending on the beam geometry and the petrology.

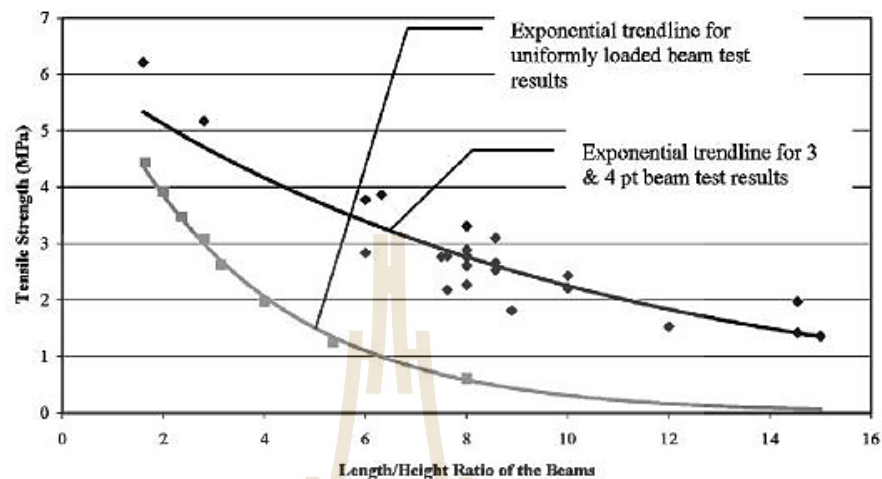


Figure 2.10 Beam tensile test results showing that the UTS is an exponential function of the beam length / height ratio (Forster, 1967 and Sen, 1961).

Liu et al. (2010) use MTS815 Flex text GT rock mechanics test system and PCI-II three-dimensional acoustic emission test system to study the damage and fractal characteristics of tensile failure in bedded salt rock are studied under indirect and direct tensile test conditions. The tensile strength as well as the correlation between indirect strength and direct tensile strength are obtained. Under indirect and direct tensile test conditions, the spatial distribution of acoustic emission and the damage evolution trend are derived for each stress stage during the full failure process. Based on the fractal column covering method, the fractal characteristic of acoustic emission spatial distribution in rock damage under indirect and direct tensile test conditions are studied. The test results indicate that indirect tensile strength of interlayer salt rock are higher than of pure salt rock and direct tensile strength of pure salt rock are much lower than

that of the indirect tensile strength. From the tensile strength difference between the indirect and direct tensile test and failure states, can tell that the tensile strength value from direct tensile test compared with the one from indirect strength test is closer to the virtual strength properties of salt rock. The research results show that with fracture dimensions of damage spatial distribution increasing, the tensile stress decreases following negative exponential law.

2.7 Loading rate effects

Zhang and Wong (2014) discussed the loading mechanisms associated with different loading rates in the bonded-particle model (BPM) and examines the numerical outputs under these different rates for used in which calibration against the results from Brazilian tensile tests have been commonly conducted. The specimens in the numerical analysis of the Brazilian tensile tests are subjected to vertical loading applied at six different loading rates: 0.005, 0.01, 0.02, 0.08, 0.2 and 0.6 m/s. The induced tensile stress σ_t is calculated as follows:

$$\sigma_t = F/\pi RT \quad (2.12)$$

where F is the compressive force acting on the platens, R and t are the radius and thickness of the Brazilian disk, respectively. The peak value of the induced tensile stress is the Brazilian tensile strength of the test specimen. The results from the Brazilian tensile tests indicate that the Brazilian tensile strength (σ_t) increases as the loading rate increases.

Wisetsaen et al. (2015) studied the effects of loading rate and temperature on tensile strength and deformation of rock salt to determine the time-dependent tensile strength and deformability of the Maha Sarakham salt under temperatures ranging from 273 to 375 K. The ring tension tests are performed under various loading rates which are equivalent to the tensile stress rates induced at the crack initiation point of 3×10^{-5} , 3×10^{-4} , 3×10^{-3} , 3×10^{-2} and 3×10^{-1} MPa/s. The results indicate that the tensile strength increases with the loading rate, and decreases with increasing temperatures.

Chobsranoi and Fuenkajorn (2016) studied the effects of loading rate on tensile strength of Maha Sarakham with various carnallite contents. The time-dependent tensile strengths of rock salt are determined with various carnallite contents ranging from 0 to 95%. The applied loading rates are varied which are equivalent to the tensile stress rates of 10^{-6} to 10^{-3} MPa/s. The results indicate that tensile strengths (σ_t) decrease when the carnallite contents ($C\%$) increase and the stress rates (σ_R) decrease, as shown in Figure 2.11.

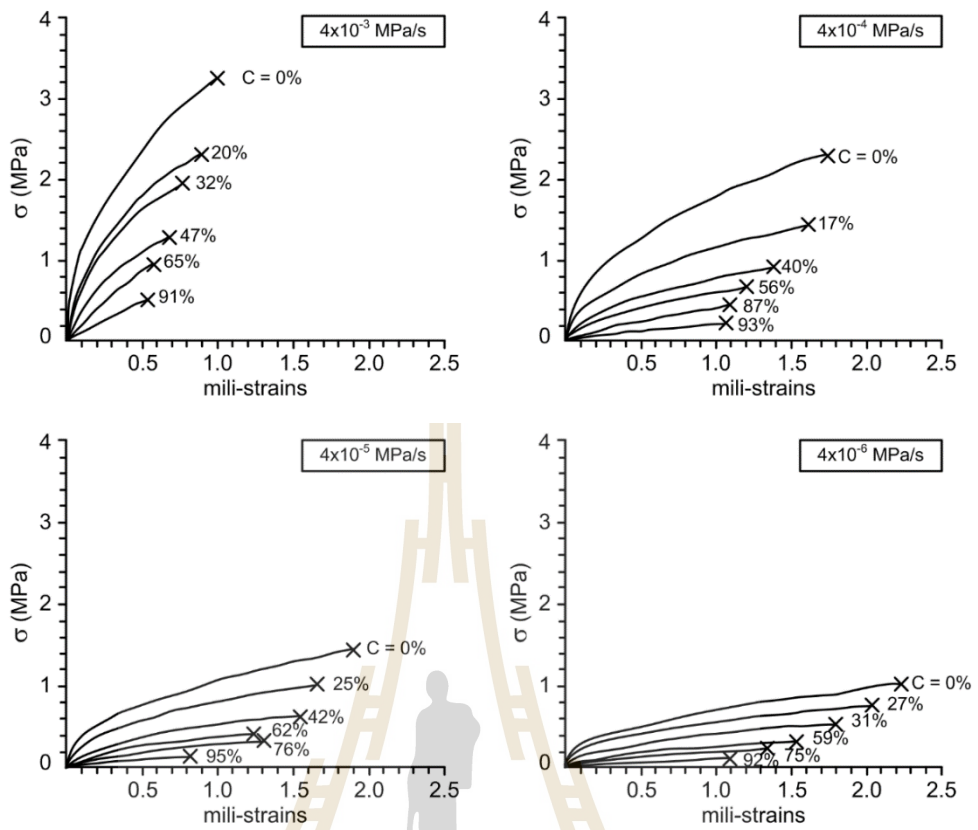


Figure 2.11 Tensile stress-strain curves for various loading rates (Chobsranoi and Fuenkajorn, 2016).

2.8 Storage in rock salt

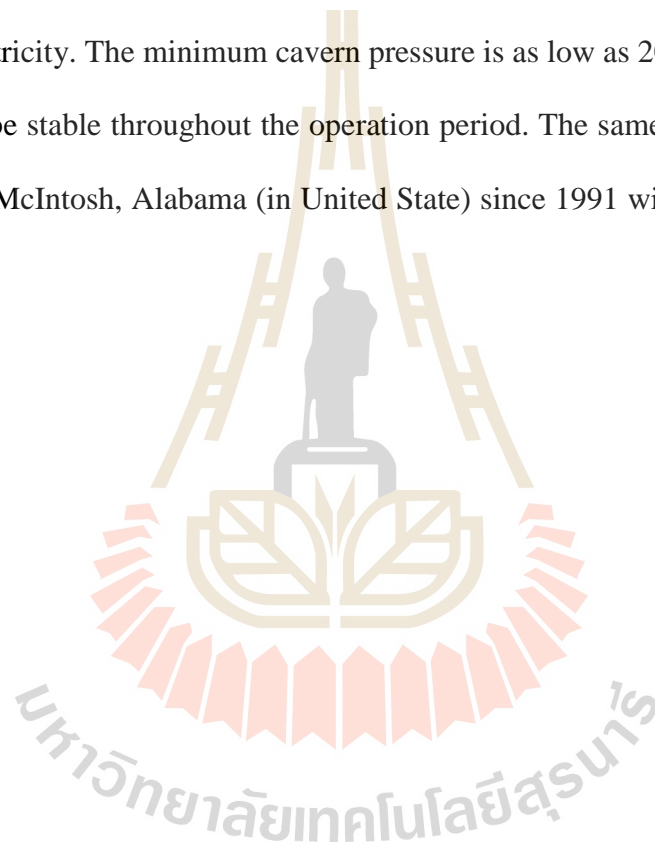
Katz and Lady (1976), Chan et al. (1980) and DeLong et al. (1989) summarize the application of CAES technology in generally. Design and analysis of the solution mined storage cavern have been comprehensively studied in the United States and Germany (Serata et al., 1989; Thoms and Martinez, 1978; Gehle and Thoms, 1986; Wittke et al., 1980, Fuenkajorn and Daemen, 1992a; Fuenkajorn and Serata, 1992). Many researchers from various organizations have studied the mechanics and geology of the underground caverns for CAES in rock salt deposits and salt domes.

Serata et al. (1989) analyze the geomechanical stability of salt dome in McIntosh, in the south of Alabama for the compressed air storage. The analysis was done by a computer model with an aid of REM software. The results from the analysis are used to assess the long-term effects on rock salt around the cavern. The analysis are also emphasized on the deformation of the cavern wall, stress distribution, the subsidence rates of ground surface, and the convergence of the cavern.

The Electric Power Research Institute (EPRI), a government organization in the United States, has conducted comprehensive research and developed the CAES technology. Various aspects have been studied and continually developed, for example, the design of an underground cavern in rock salt deposits (EPRI, 1990a: 1990b: 1990c: 1992a: 1992b; 1992c: 1994a: 1994b), design of power generator for CAES (EPRI, 1994c: 1994e: 1997: 1999), economic assessment (EPRI, 1986; 1999), and CAES for other types of underground media. Due to copyrights restrictions as well as commercial competition, the results of these studies have not been published.

The first compressed air energy storage (CAES) in the world is the Huntorf Plant in Germany which was started in 1978 (Crotogino et al., 2001). The plant with

290 MW of power consists of two underground caverns that contains a total volume of 310,000 cubic meters. The caverns are situated 220 meter apart. The caverns ceilings are at 650 meters deep from the ground surface. The constant volume system is employed to reconvert the compressed air to produce electricity. Air is compressed into the cavern at the rate of approximately 108 kg/sec. The maximum allowable pressure in the cavern is 70 bar. The compressed air is released with the rate of 417 kg/sec to produce electricity. The minimum cavern pressure is as low as 20 bar. The caverns are designed to be stable throughout the operation period. The same technology has been also used in McIntosh, Alabama (in United State) since 1991 with the power capacity of 110 MW.



CHAPTER III

SAMPLE PREPARATION

3.1 Introduction

This chapter describes the rock salt sample preparation procedure to be used in the four point bending test.

3.2 Sample preparation

The tested specimens have been obtained from the underground openings of ASEAN Potash Chaiyaphum Co., Ltd. (APOT). They belong to Lower Salt member of the Maha Sarakham formation. Warren (1999) describes the origin and geological structures of the Maha Sarakham salt. The specimens used for four-point bending tests are prepared as prismatic blocks with nominal dimensions of $50 \times 50 \times 200 \text{ mm}^3$ (Figures 3.1 and 3.2). Sets of the specimens are prepared for compression-to-tension cyclic loading (CTC) tests. Figure 3.3 shows example of the specimen with strain gage (TML, PFL-20-11-1L, 20 mm) installed at the crack initiation point. The bedding planes are parallel to the specimen main axis and normal to the loading directions. The average density is 2.13 g/cc. The tested specimens comprise mainly of NaCl with slight amount (less than 1%) of ferrous oxides.

The ratio of specimen length to specimen diameter (L/D) is 4.0. Twelve salt specimens are prepared for cyclic loading tests. Table 3.1 shows the summary of salt specimen dimensions.

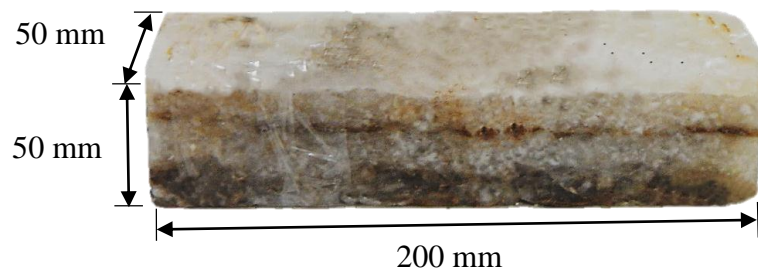


Figure 3.1 Example of prismatic salt specimens with nominal dimensions of $50 \times 50 \times 200 \text{ mm}^3$.

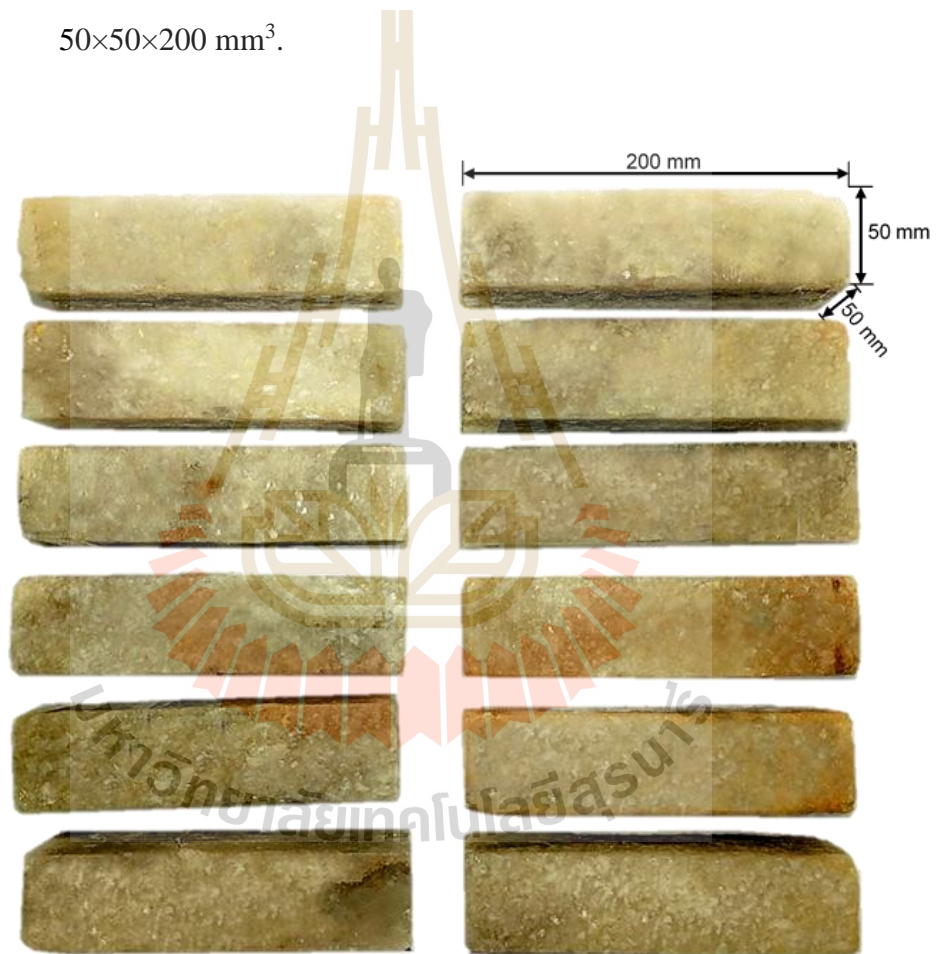


Figure 3.2 Some salt specimens prepared for four point bending test with $L/D = 4$.

3.3 Strain gage installation

A strain gage (TML, PFL-20-11-1L, 20 mm) is installed to measure tensile strains at the center of the specimen in horizontal. The main axis of the specimen is parallel to the bedding planes (Figure 3.3). Gage length is 20 mm. and gage factor is $2.13 \pm 1\%$.

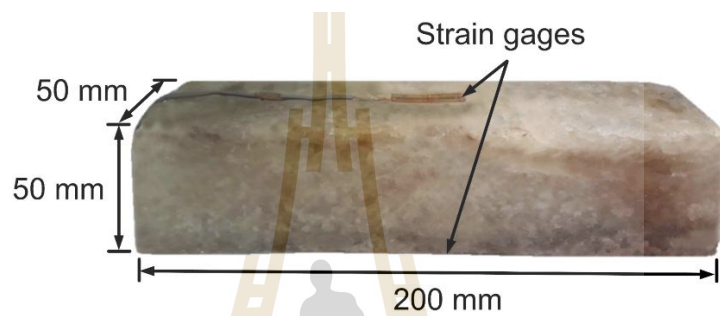


Figure 3.3 Example of prismatic salt specimen with strain gage position salt specimens prepared for four point bending test.

Table 3.1 Salt specimens prepared for cyclic loading tests.

Specimen Number	Average Width (mm)	Average Height (mm)	Average Length (mm)	Weight (g)	Density (g/cc)
RS-Cyclic-01	50.70	50.28	200.70	1098.97	2.15
RS-Cyclic-02	50.18	50.60	197.30	1048.57	2.09
RS-Cyclic-03	50.84	49.00	200.00	1080.55	2.17
RS-Cyclic-04	50.00	49.74	198.84	1053.63	2.13
RS-Cyclic-05	50.00	50.40	201.00	1073.66	2.12
RS-Cyclic-06	49.94	50.10	199.82	1045.02	2.09
RS-Cyclic-07	50.20	49.06	200.34	1024.29	2.08
RS-Cyclic-08	50.00	49.98	200.24	1043.53	2.09
RS-Cyclic-09	50.30	50.38	199.92	1076.82	2.13
RS-Cyclic-10	49.28	50.30	202.40	1084.62	2.16
RS-Cyclic-11	50.58	50.38	200.60	1116.78	2.18
RS-Cyclic-12	50.48	51.00	201.80	1118.12	2.15
Mean ± SD					2.13 ± 0.04

CHAPTER IV

LABORATORY TESTING METHOD

4.1 Introduction

The objective of four-point bending test is to determine the maximum tensile stress of rock salt under compression-to-tension loading cycles. This chapter describes the test methods of the bending tensile tests of the Maha Sarakham salt under various loading configurations. The testing procedures and equipment are also described.

4.2 Test method

The four-point bending test method and calculation follow the ASTM standard practice (D6272-10). Figure 4.1 shows the loading directions for the compression-to-tension cyclic loading (CTC) testing. The load directions are normal to the bedding planes. A data logger (TC-32K) connected with the switching box (Type B-2760) is used to monitor the induced compressive and tensile strains while loading (Figure 4.2). The bending stress is calculated by Gere (2004):

$$\sigma = My / I \quad (4.1)$$

where σ is bending stress along y-axis throughout the cross section, M is bedding moment, y is distance from the neutral axis to the given point of the cross section and I is moment of inertia.

This flexure formula shows that the stresses are directly proportional to the bending moment M and inversely proportional to the moment of inertia I of the cross section. The stresses vary linearly with the distance y from the neutral axis, as shown in Figure 4.3.

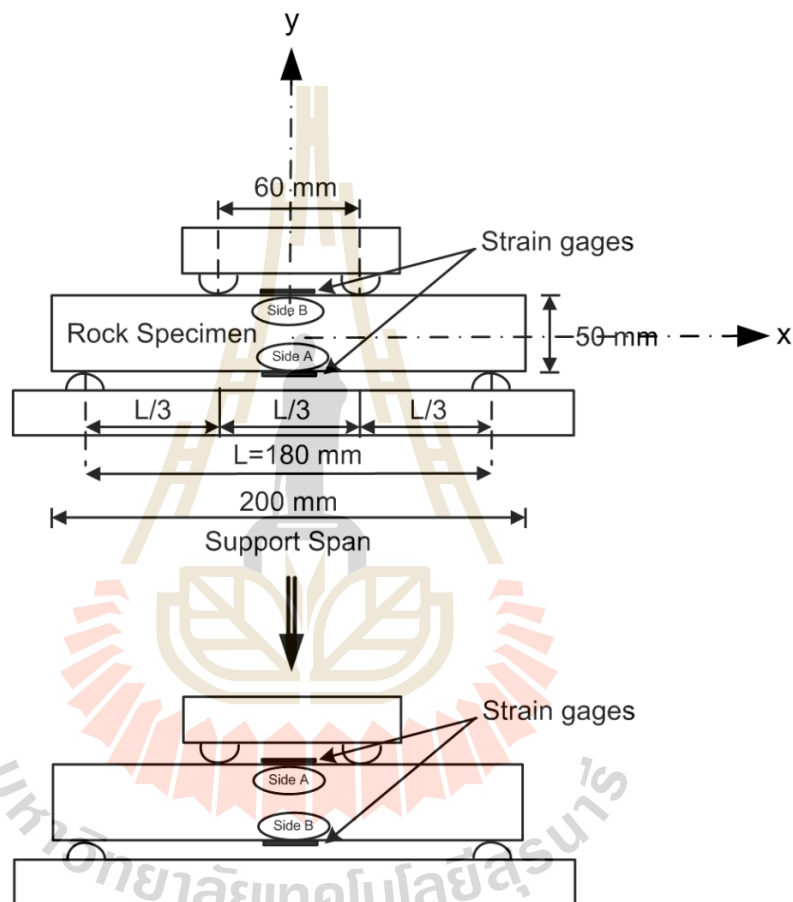


Figure 4.1 Test arrangement for four-point bending test (ASTM (D6272-10) under compression-to-tension loading.

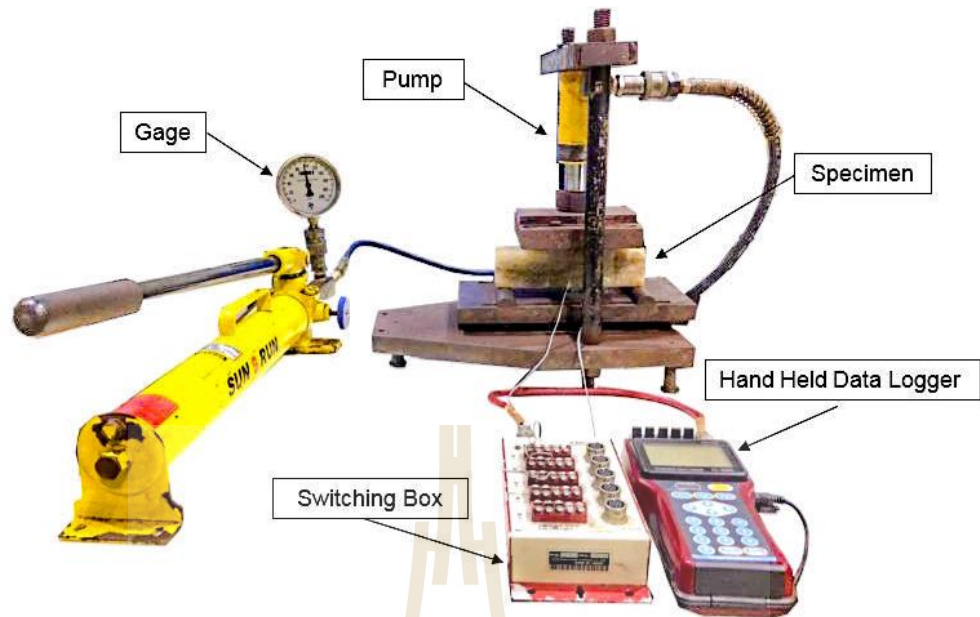


Figure 4.2 Four point bending test apparatus.

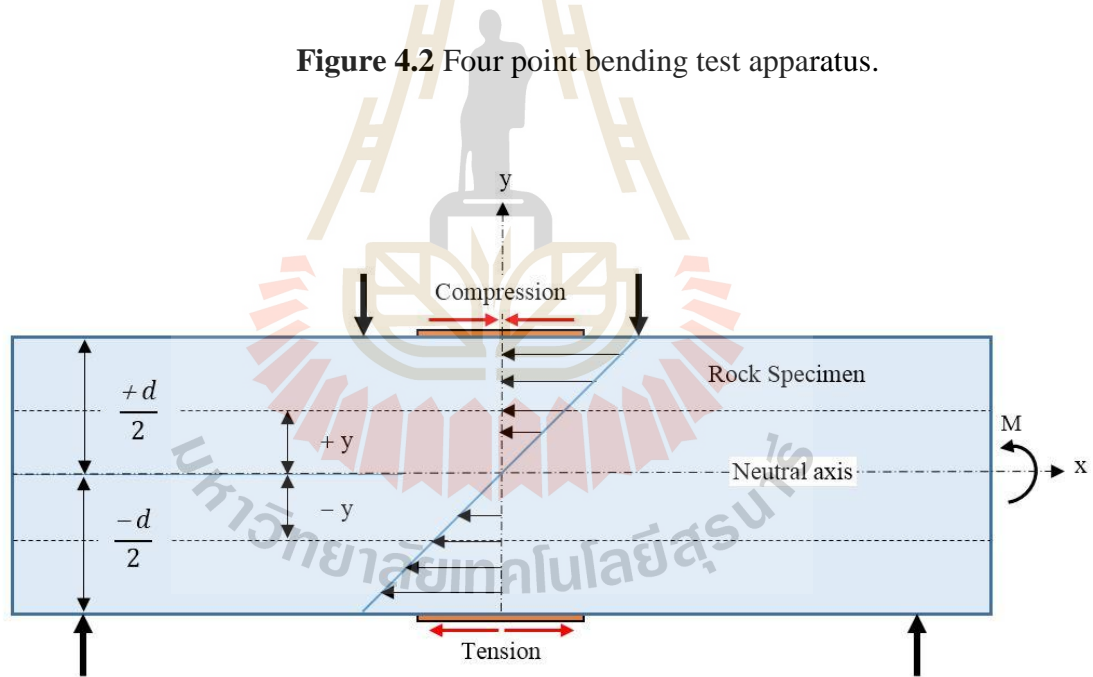


Figure 4.3 Stress distribution at mid-section of specimen.

The stress will also have the correct signs (tension is negative, compression is positive), as distance y is positive if the point lies above the neutral axis and negative if it lies below the neutral axis.

For a rectangular sample under a load in a four-point bending setup where the loading span is one-third of the support span (Figure 4.1):

$$M = PL/6 \quad (4.2)$$

$$I = bd^3/12 \quad (4.3)$$

where M is bedding moment, P is the applied load, L is nominal length, I is moment of inertia, b is nominal width, and d is nominal thickness.

Substituting Equations (4.2) and (4.3) into Equation (4.1) the proposed stress in the outer fiber throughout the load span can be presented in form of the compressive stress and tensile stress along the beam (rock stresses), as follows:

$$\sigma = 2yPL/bd^3 \quad (4.4)$$

where y is distance from the neutral axis to the given point of the cross section (Figure 4.3).

The maximum compressive stress is obtained when $y_{\max} = + d/2$, the under maximum tensile stress is obtained when $y_{\max} = - d/2$.

$$\sigma_c = + PL/bd^2 \quad (4.7)$$

$$\sigma_t = - PL/bd^2 \quad (4.8)$$

where σ_c is maximum compressive stress, σ_t is maximum tensile stress, y is distance from the neutral axis to the given point of the cross section, L is nominal length span (180 mm), b is nominal width (50 mm), and d is nominal thickness (50 mm).

The cyclic loading is applied until tensile failure is induced on either side of specimen. The designed maximum tensile stresses for each test series of cyclic loading are 0.40, 0.60, 0.80, 1.00, 1.20 and 1.40 MPa. The loading frequencies are 0.1 and 1 MHz. The loading-unloading frequencies and amplitudes of the applied load are controlled by a pressure pump. Once the defined tensile stresses are reached, the sample is flipped over to obtain the alternate compression-to-tension loading, as shown in Figure 4.1.

CHAPTER V

TEST RESULTS

5.1 Introduction

The test results obtained from four point bending under compression-to-tension cyclic loading are described in this chapter. They are presented in the forms of stress-strain curves, and S-N (fatigue) curves. Post-test observations and the effects of cyclic loading on the tensile elastic modulus of the salt are also presented.

5.2 Four point bending with cyclic loading test results

The tensile stress-strain curves measured during cyclic loading tested specimens are shown in Figure 5.1. The number of loading cycles increases with decreasing the maximum applied stresses (amplitudes) and loading frequencies. The accumulated strains at failure clearly increase as the amplitudes and loading frequencies are decreased. Table 5.1 and Figure 5.2 summarize the maximum tensile stresses, accumulated strains at failure, tensile elastic modulus and maximum number of cycle for all tested specimens. The elastic modulus decreases with increasing applied maximum stresses and loading frequencies.

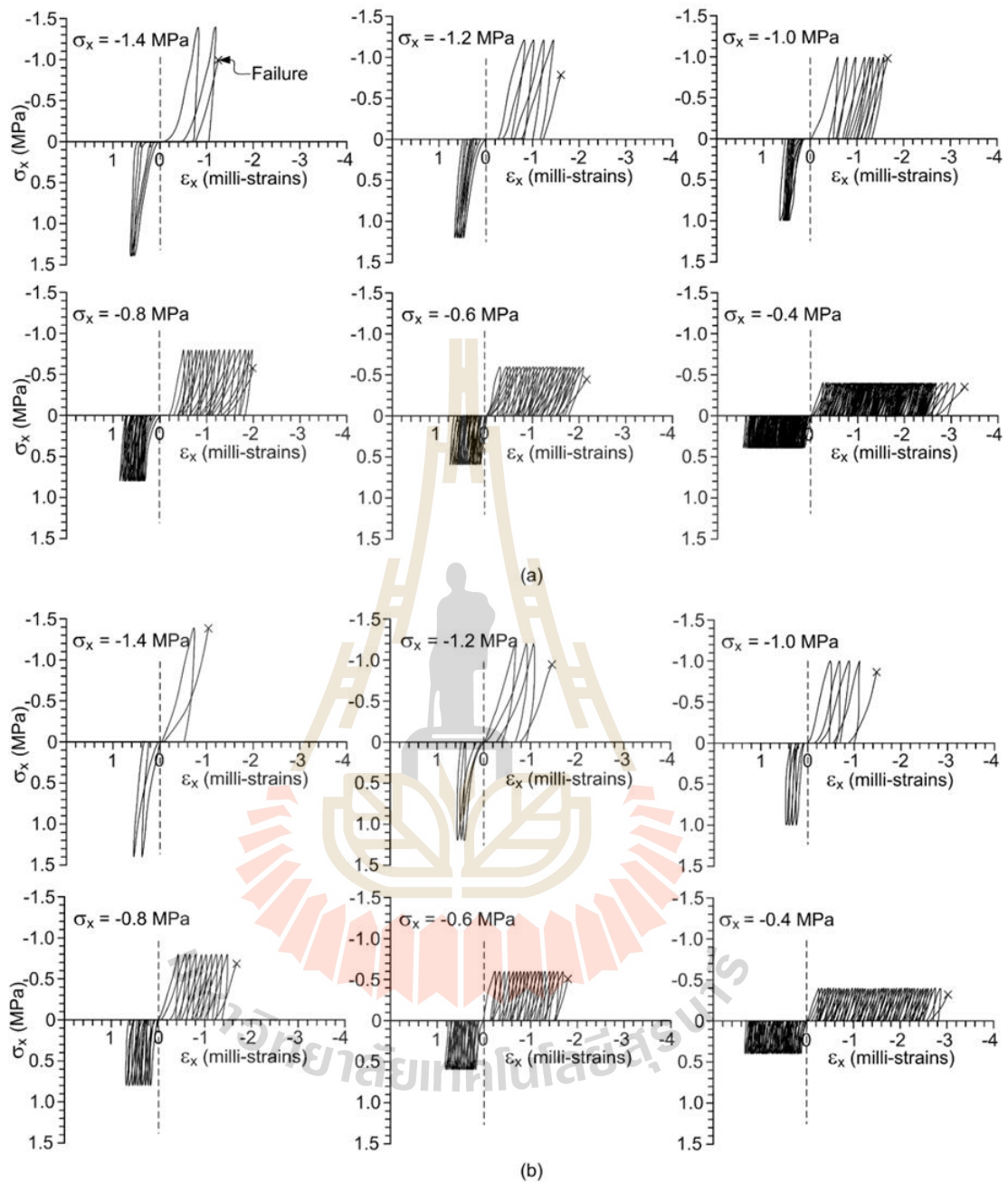


Figure 5.1 Compressive and tensile stresses (σ_x) as a function of compressive and tensile strains (ϵ_x) at failure surface (upper or lower side) measured for cyclic loading at $f = 1$ mHz (a) and at $f = 0.1$ mHz (b).

Table 5.1 Cyclic loading tests results.

Loading configurations	f (mHz)	σ_x (MPa)	ϵ_x (milli-strains)	E_0 (MPa)	N
Cyclic loading	1.0	-1.40	-1.27	1.35	2
		-1.20	-1.62	1.31	4
		-1.00	-1.68	0.84	7
		-0.80	-1.99	1.14	17
		-0.60	-2.14	1.02	25
		-0.40	-3.33	0.80	91
	0.1	-1.40	-1.08	1.95	1.5
		-1.20	-1.47	0.95	2
		-1.00	-1.57	0.93	4
		-0.80	-1.67	0.96	10
		-0.60	-1.85	1.72	18
		-0.40	-3.04	0.77	46

Figure 5.2 plots the fatigue tensile stresses (σ_x) as a function of loading cycles, e.g. S-N curves. The effect of loading frequencies tends to be relatively small. The lower frequencies tend to induce lower fatigue stress.

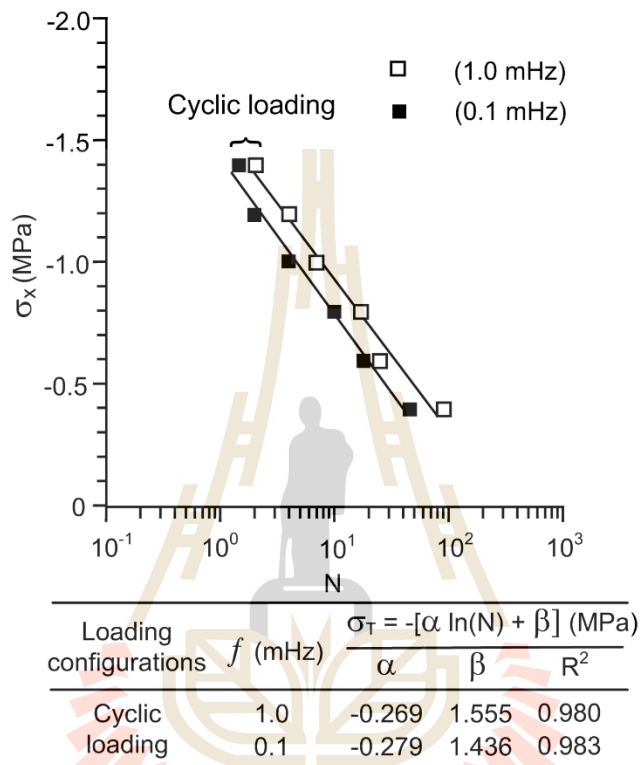
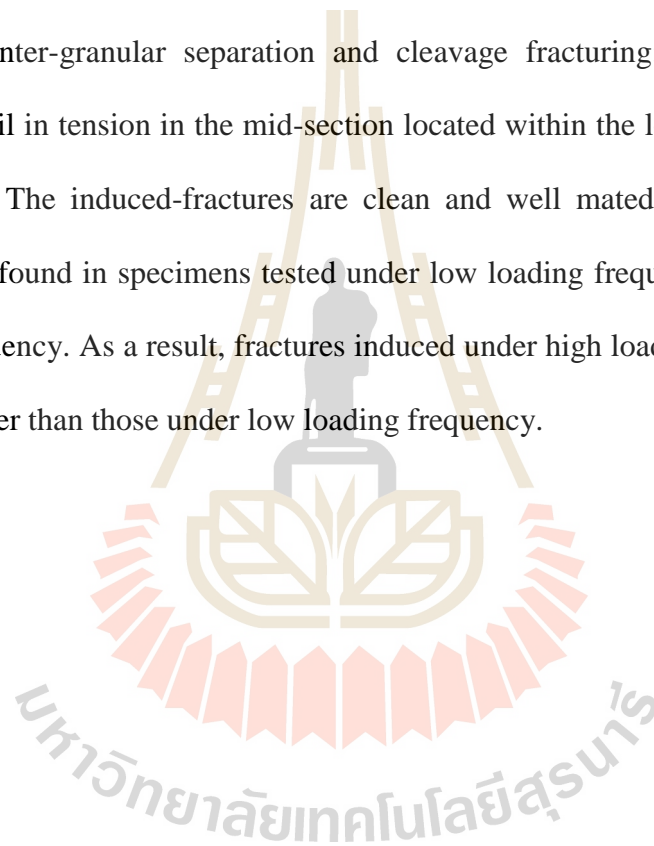


Figure 5.2 Fatigue tensile stress (σ_T) as a function of loading cycles.

Figure 5.3 shows the normalized tensile elastic modulus (E/E_0) plotted as a function of a number of loading cycles, where E_0 is the tensile elastic modulus obtained at the first cycle. The normalized elastic modulus rapidly decreases with increasing loading cycles. The specimens tested under low loading frequencies show the normalized elastic modulus lower than those under high frequencies. Post-failure observations of cyclic specimens show that there are two modes fracturing in the specimens: inter-granular separation and cleavage fracturing: (Figures 5.4). All specimens fail in tension in the mid-section located within the load span, as shown in Figure 5.5. The induced-fractures are clean and well mated. More inter-granular fracturing is found in specimens tested under low loading frequency than under high loading frequency. As a result, fractures induced under high loading frequency appear to be smoother than those under low loading frequency.



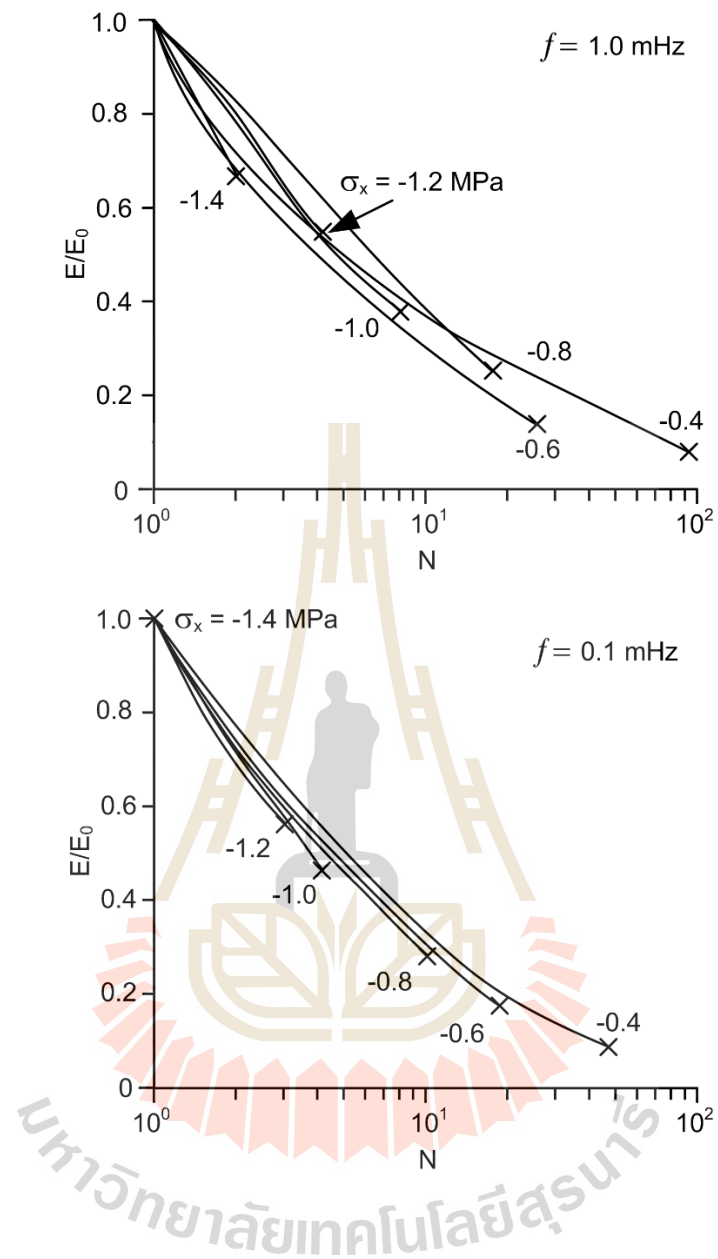


Figure 5.3 Normalized tensile elastic modulus (E/E_0) plotted as a function of number of loading cycles (N) up to failure for cyclic loading tests.

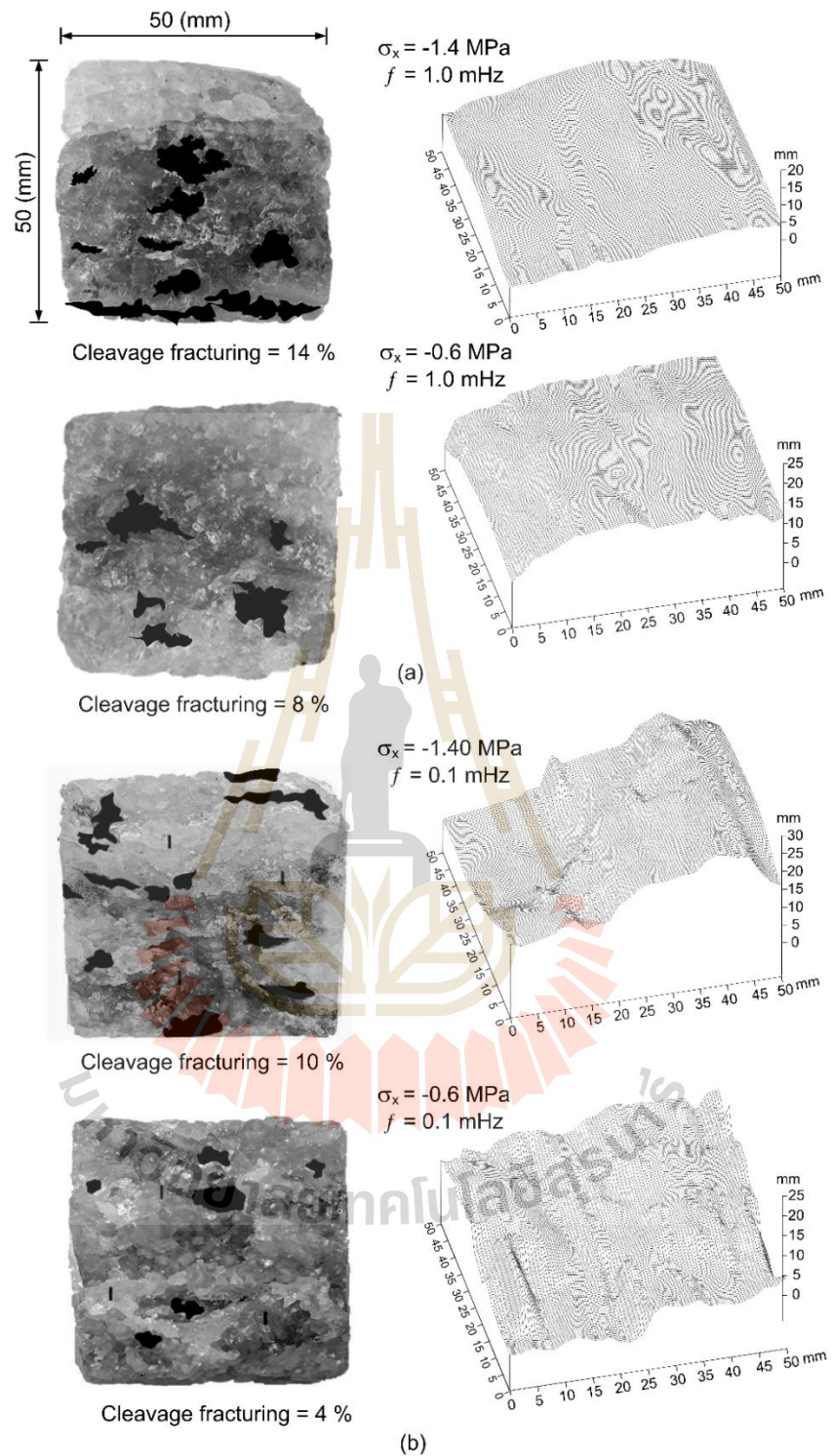


Figure 5.4 Fracture surfaces and their laser-scanning profiles for high loading frequencies (a), and for low loading frequencies (b). Cleavage fracturing highlighted in dark area.

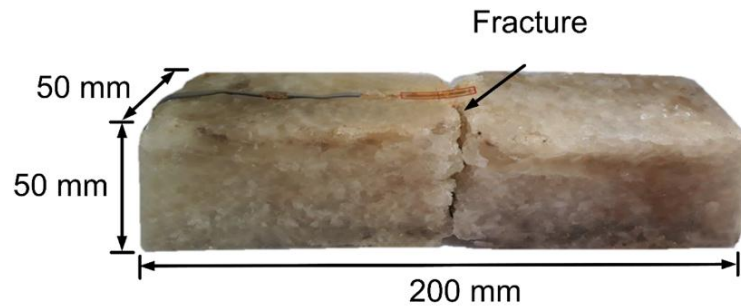


Figure 5.5 Some post-test specimens of Maha Sarakham salt obtained from four point bending testing under cyclic loading test.

The time-dependent behaviour of salt specimens as determined under cyclic loading test from 0.4, 0.6, 0.8, 1.0, 1.2 and 1.4 MPa. The loading frequencies are 0.1 and 1.0 mHz. Table 5.2 show the applied load and loading frequencies. The results are presented in forms of loci of maximum tensile strains (ϵ_t) and compressive strains (ϵ_c) as a function of time. It can be interpreted as hysteresis loops compaction and hardening behaviour of specimens. This is because the salt behave as a strain-hardening material. Figures 5.6 through 5.9 show the tensile strain-time curves complied from loci of the loading cycles by plotting the maximum point of each cycles. The curves show the transient, steady-state and tertiary creep phases which are similar to those obtained from static creep testing. The cyclic loading test results indicate that the maximum number of loading cycles increases with decreasing the maximum applied stresses (amplitudes). Similar behaviour also observed from the compression cyclic loading test results obtained by Fuenkajorn and Phueakphum (2010). The accumulated tensile strain, fatigue tensile stresses and time are monitored during loading. Plots strain-time curves from cyclic loading tests. The specimens tested under higher tensile stresses show larger cyclic strains at failure. The visco-plastic coefficient of each specimen will be

calculated by assuming that the salt behaved as a Burgers material to compare with the static loading tests in the next chapter.

Table 5.2 The results are constant stresses under cyclic loading test.

Loading configurations	Cyclic loading test	f	σ_x	Time	ϵ_c @ Side	ϵ_t @ Side	ϵ_c @ Side	ϵ_t @ Side
		(mHz)	(MPa)	(hour)	A (milli- strains)	A (milli- strains)	B (milli- strains)	B (milli- strains)
		1	-1.40	0.36	0.63	-1.27	0.62	-1.22
			-1.20	0.69	0.68	-1.62	0.61	-1.49
			-1.00	1.38	0.66	-1.38	0.65	-1.68
			-0.80	2.86	0.83	-1.99	0.77	-1.65
			-0.60	4.20	0.80	-1.50	0.81	-2.14
			-0.40	15.04	1.12	-2.65	1.47	-3.23
		0.1	-1.40	2.06	0.56	-1.08	0.51	-1.00
			-1.20	5.31	0.56	-1.01	0.56	-1.47
			-1.00	7.00	0.50	-1.04	0.60	-1.57
			-0.80	17.00	0.74	-1.38	0.67	-1.67
			-0.60	30.36	0.79	-1.85	0.75	-1.68
			-0.40	75.36	1.51	-2.58	1.29	-3.04

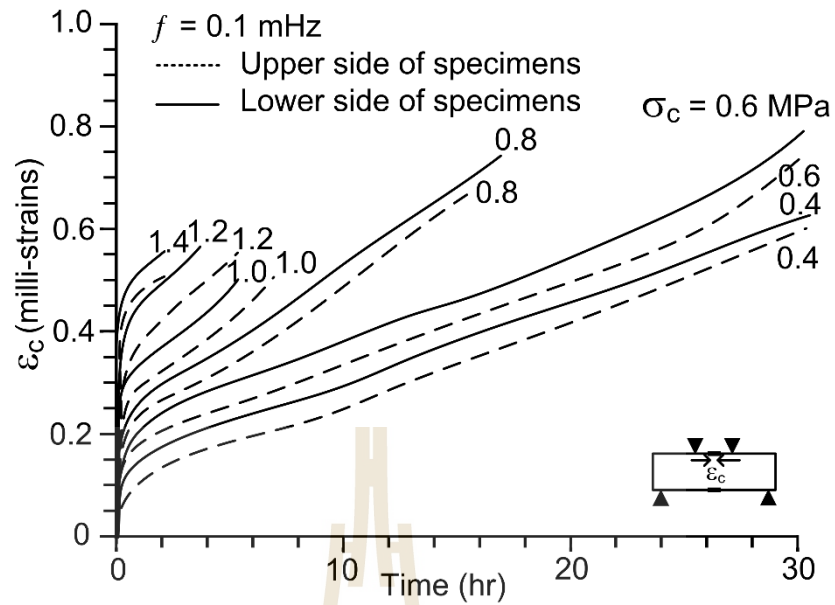


Figure 5.6 Compressive strain (ϵ_c) as a function of time for cyclic loading tests at

$f = 0.1$ mHz.

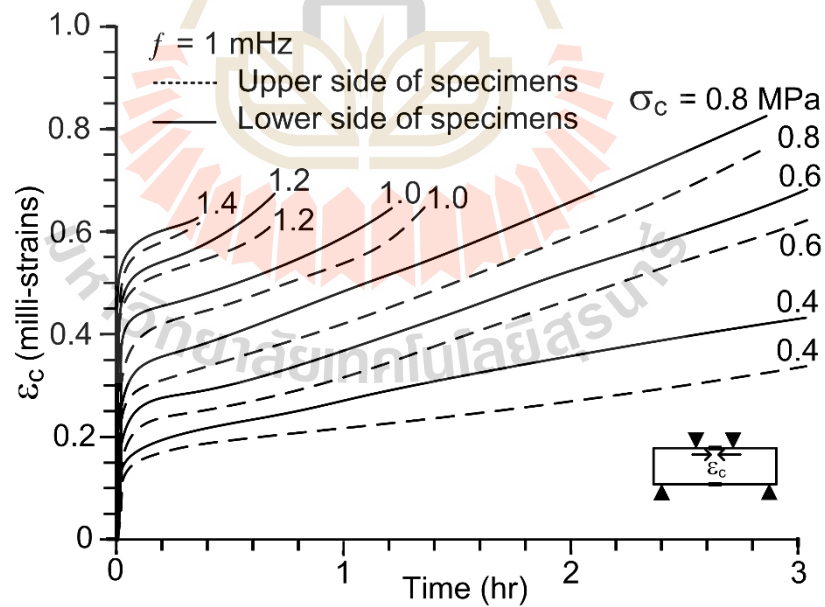


Figure 5.7 Compressive strain (ϵ_c) as a function of time for cyclic loading tests at

$f = 1.0$ mHz.

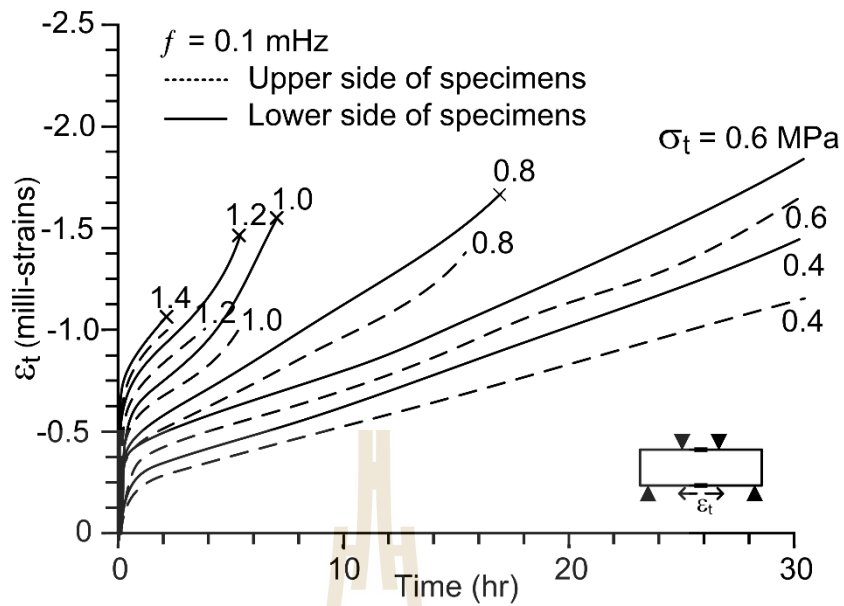


Figure 5.8 Tensile strain (ϵ_t) as a function of time for cyclic loading tests at $f = 0.1$ mHz.

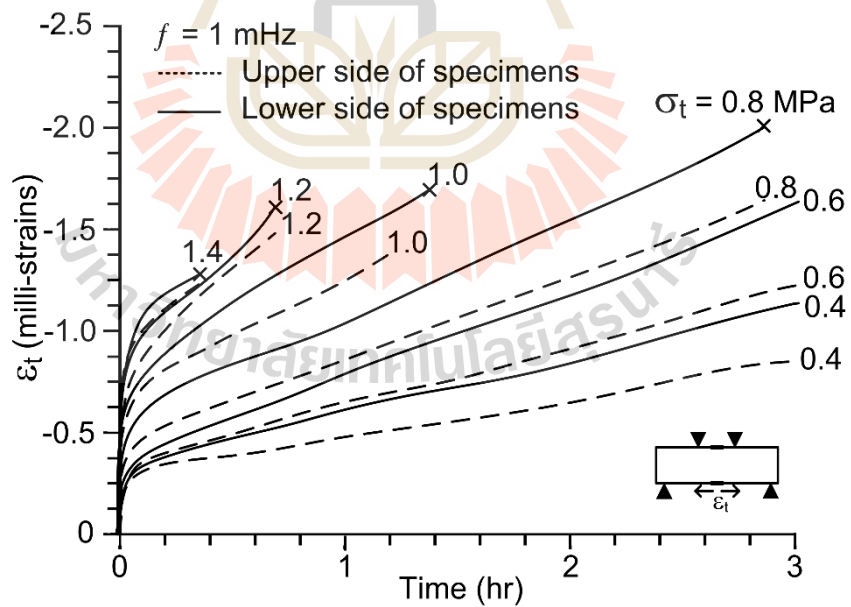


Figure 5.9 Tensile strain (ϵ_t) as a function of time for cyclic loading tests at $f = 1.0$ mHz.

CHAPTER VI

ANALYSIS OF TEST RESULTS

6.1 Introduction

The purpose of this chapter is to analyze the results obtained here and compare with the tension cyclic loading (TC) that was obtained by Plangklang (2017). The compression is made in terms of S-N curves and the normalized tensile elastic modulus (E/E_0) as a function of a number of loading cycles. Loci of the strain-time curves are plotted to show the transient, steady-state and tertiary creep phases. The Burgers model is used to fit these curves.

6.2 Analysis

The tensile stress-strain curves measured during loading TC tested specimens of Plangklang (2017) are given in Figure 6.1 (a) and for compression-to-tension (CTC) tested specimens in Figure 6.1 (b). Table 6.1 summarizes the maximum tensile stresses, accumulated strains at failure, tensile elastic modulus and maximum number of loading cycles for all tested specimens. Under CTC loading the salt specimens can accumulate the tensile strains more quickly than those under TC loading. The elastic modulus (at the first cycle) of CTC tested specimens is slightly lower than those of TC tested specimens. It seems that the salt specimens subjected to CTC loading can sustain much less maximum stresses and loading cycles than those under TC loading. The decrease of the failure (fatigue) stresses as a function of loading cycle (N) can be represented by a logarithmic equation as

$$\sigma_T = -[\alpha \ln(N) + \beta] \quad (\text{MPa}) \quad (6.1)$$

where σ_T is fatigue tensile stress, N is loading cycle, α and β are empirical parameters used to calculate the fatigue tensile strengths. Regression analysis is performed to determine the constants α and β . Their numerical values are given in Figure 6.2. The accumulated tensile strains (ϵ_t) at failure are plotted as a function of loading cycles in Figure 6.3. The diagrams also suggest that under CTC loading the salt specimens can accumulate the tensile strains more quickly than those under TC loading.

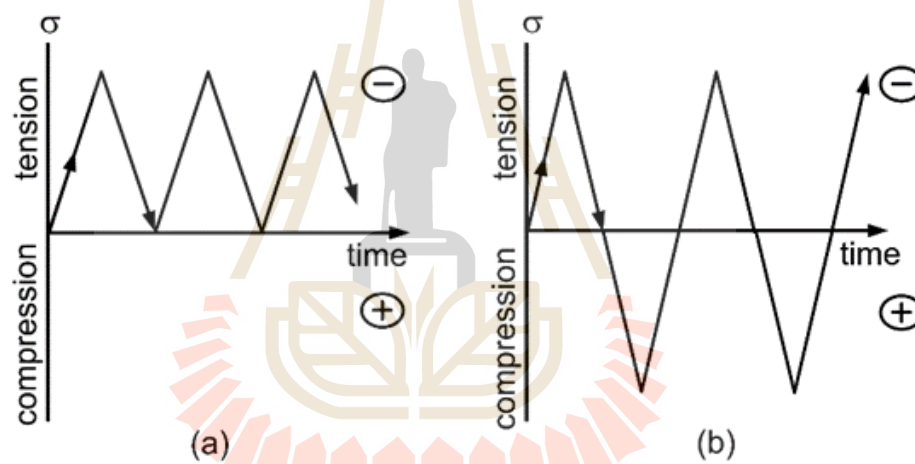


Figure 6.1 Cyclic loading paths for TC loading (a) (Plangklang, 2017) and CTC loading (b) used in this study.

Table 6.1 Cyclic loading tests results of TC loading tests (Plangklang, 2017) and CTC loading tests.

Loading configurations	f (mHz)	σ_x (MPa)	ϵ_x (milli-strains)	E_0 (MPa)	N
TC	10	-3.20	-0.78	-	0.5
		-2.80	-1.09	1.64	7
		-2.55	-1.25	1.38	15
		-2.40	-1.32	1.68	17
		-2.24	-1.38	1.79	55
		-1.99	-1.46	1.91	62
		-1.87	-1.58	1.77	810
	1	-1.22	-1.99	1.39	4,814
		-2.90	-0.76	-	0.5
		-2.56	-1.03	1.24	6
		-2.40	-1.10	1.18	10
		-2.25	-1.19	1.34	27
		-1.99	-1.33	1.11	42
		-1.88	-1.53	1.26	281
-1.40	-1.54	1.46	1,021		
CTC	1	-1.40	-1.27	1.35	2
		-1.20	-1.62	1.31	4
		-1.00	-1.68	0.84	7
		-0.80	-1.99	1.14	17
		-0.60	-2.14	1.02	25
		-0.40	-3.33	0.80	91
		-1.40	-1.08	1.95	1.5
	0.1	-1.20	-1.47	0.95	2
		-1.00	-1.57	0.93	4
		-0.80	-1.67	0.96	10
		-0.60	-1.85	1.72	18
		-0.40	-3.04	0.77	46

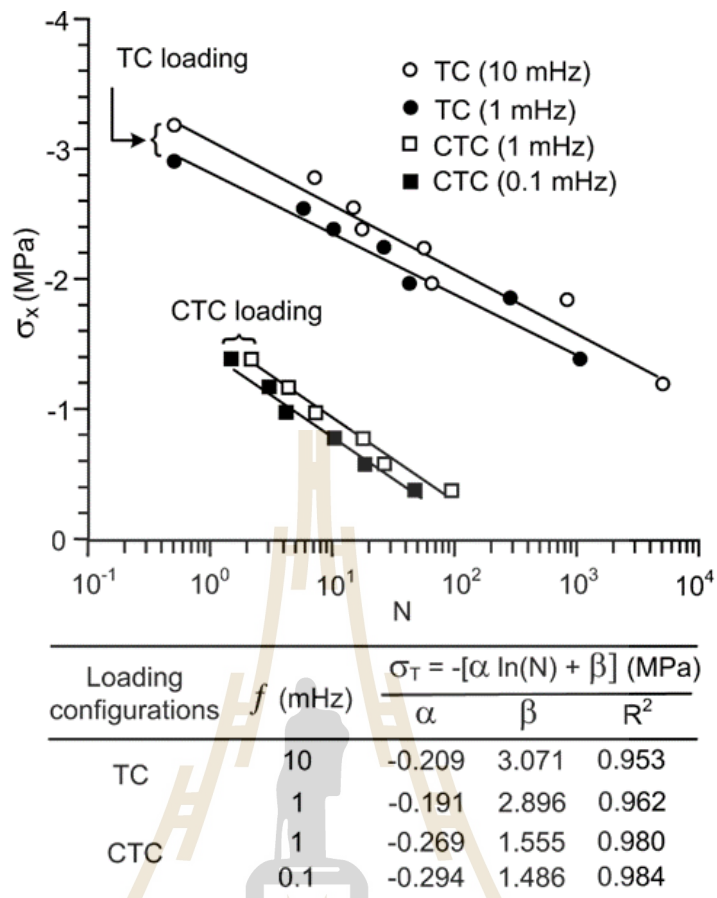


Figure 6.2 Fatigue tensile stress (σ_T) as a function of number of loading cycles at failure (N) for TC (Plangklang, 2017) and CTC tests.

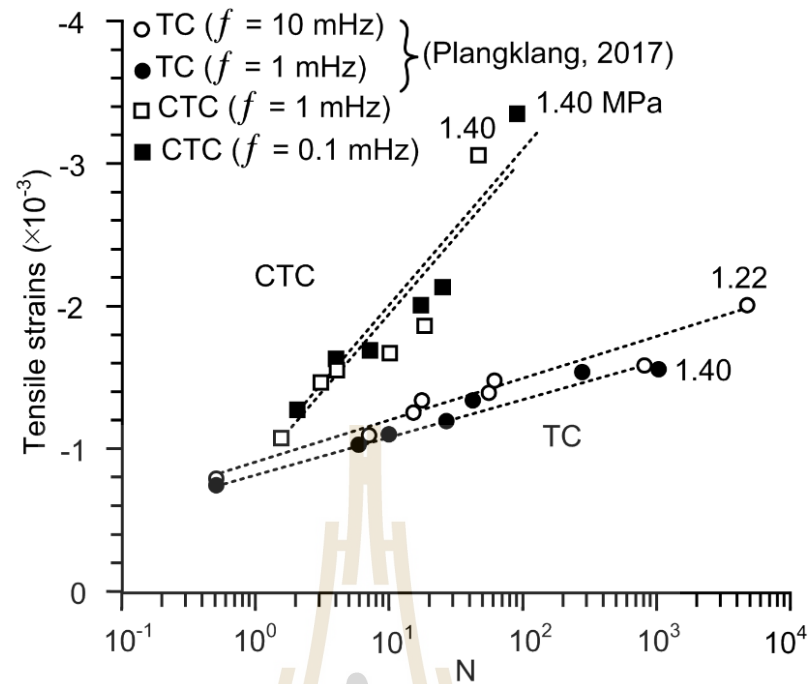


Figure 6.3 Fatigue tensile strains as a function of number of loading cycles (N) for TC (Plangklang, 2017) and CTC tests.



Figure 6.4 and Table 6.1 show the normalized tensile elastic modulus (E/E_0) plotted as a function of a number of loading cycles for the TC and CTC testing. The CTC testing gives the normalized elastic modulus values lower than the TC testing. The non-linear relation is observed for CTC testing, particularly under low loading frequencies.

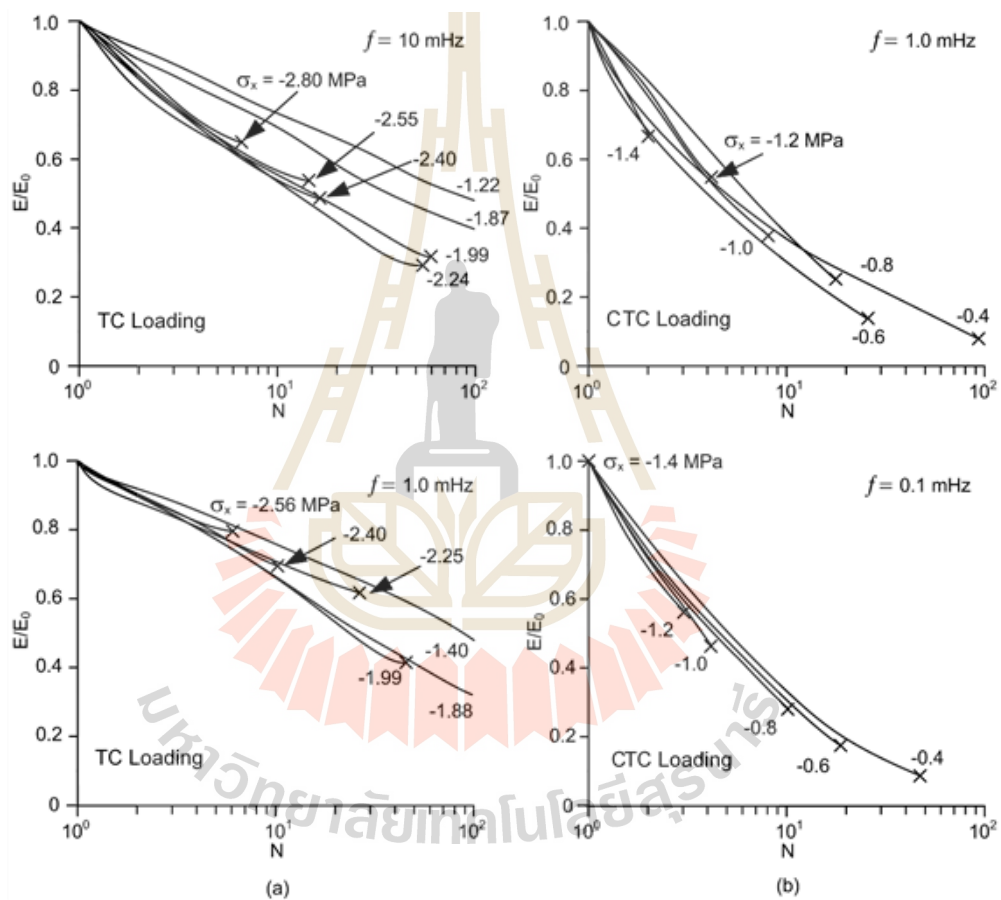
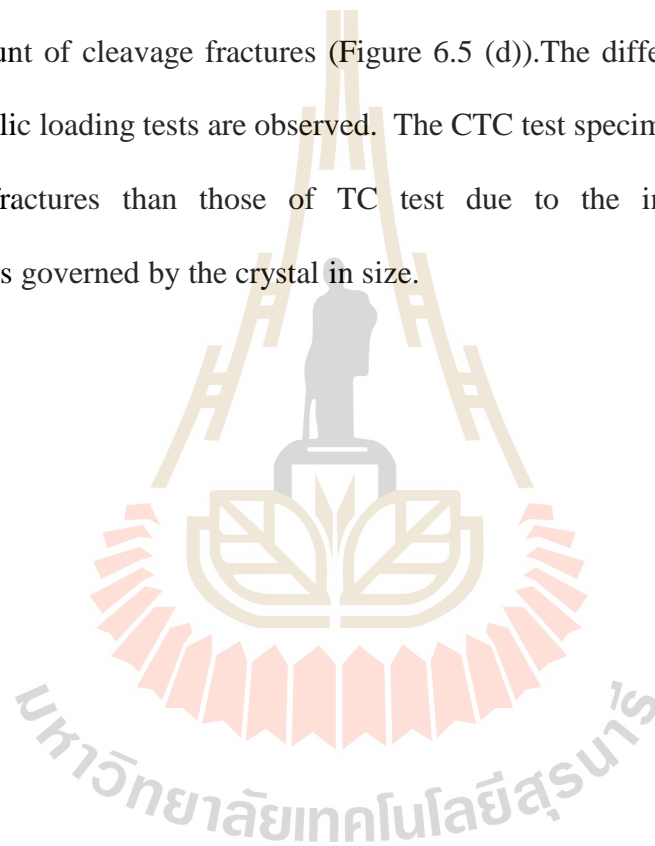


Figure 6.4 Normalized tensile elastic modulus (E/E_0) plotted as a function of number of loading cycles (N) up to failure for TC loading tests (a) by Plangklang (2017) and CTC loading tests (b).

Post-failure observations of cyclic specimens show that there are two types of fracturing in the specimens: cleavage fracturing (splitting of salt crystals at the cleavage planes) and inter-granular fracturing (Figure 6.5). Post-test specimens of TC test show cleavage fracturing distributed in the fracture area, particularly under the high loading frequencies, as shown in Figure 6.5 (a) that was tested by Plangklang (2017). More inter-granular fracturing is found in specimens tested under CTC test, accompanied by a small amount of cleavage fractures (Figure 6.5 (d)). The different surface fractures from two cyclic loading tests are observed. The CTC test specimens show more rough and sharp fractures than those of TC test due to the inter-granular fracture characteristics governed by the crystal in size.



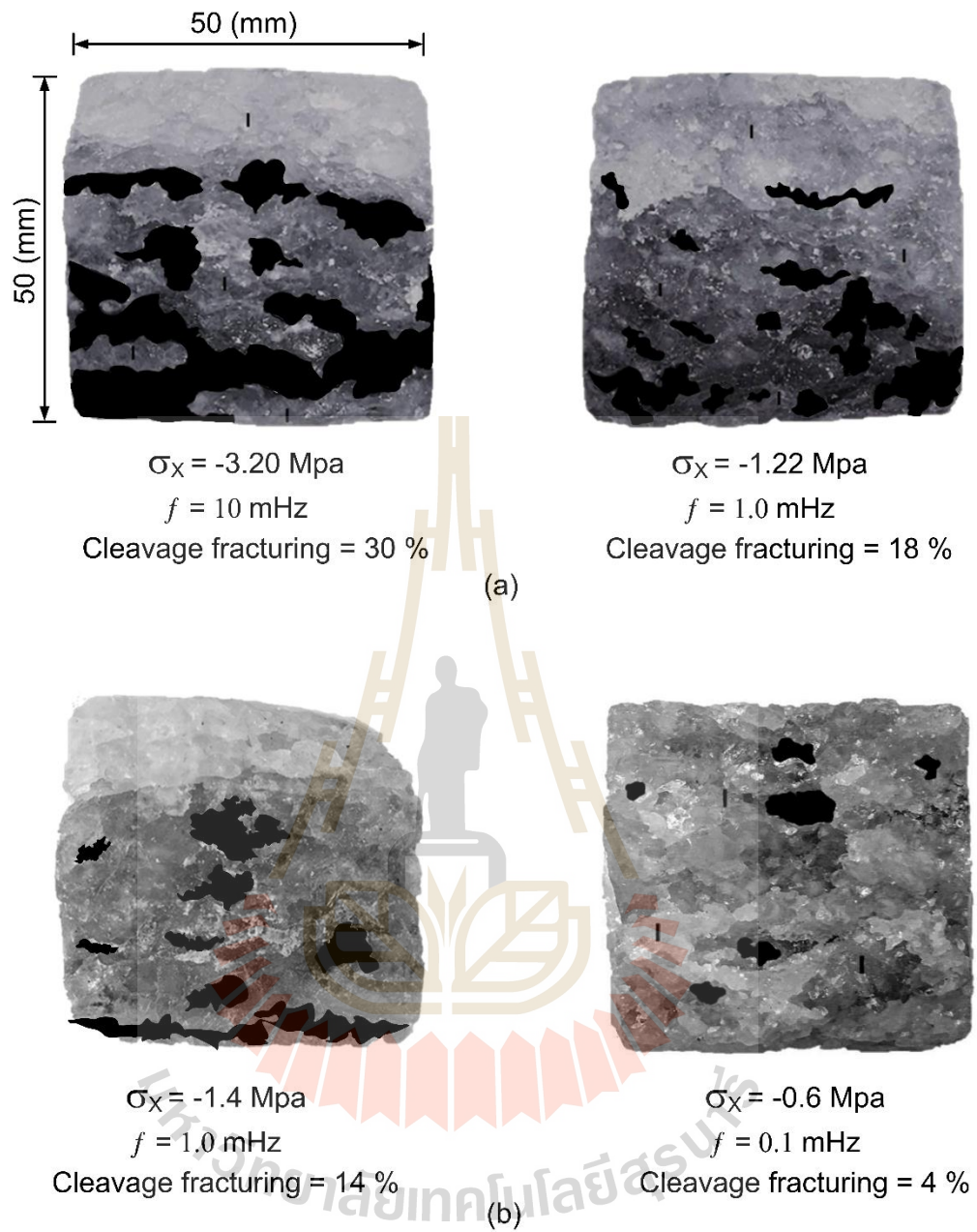


Figure 6.5 Fracture surfaces and their laser-scanning profiles for TC test (a)

(Plangklang, 2017), and for CTC test (b).

The Burgers model (Richard, 1993) is used to describe the time-dependent deformation of the creep test specimens. It is recognized that numerous creep models or constitutive equations have been developed to represent the time-dependent behavior of rock salt (e.g., Gnirk and Johnson, 1964; Senseny, 1984; Handin et al., 1984; Langer, 1984; Hardy and Sun, 1986).

The Burgers model is used here because it is simple and capable of describing the tensile elastic, visco-elastic and visco-plastic phases of deformation. Assuming that the salt is isotropic and linearly elastic a relation between tensile strain and stress can be written as (Jaeger et al., 2007):

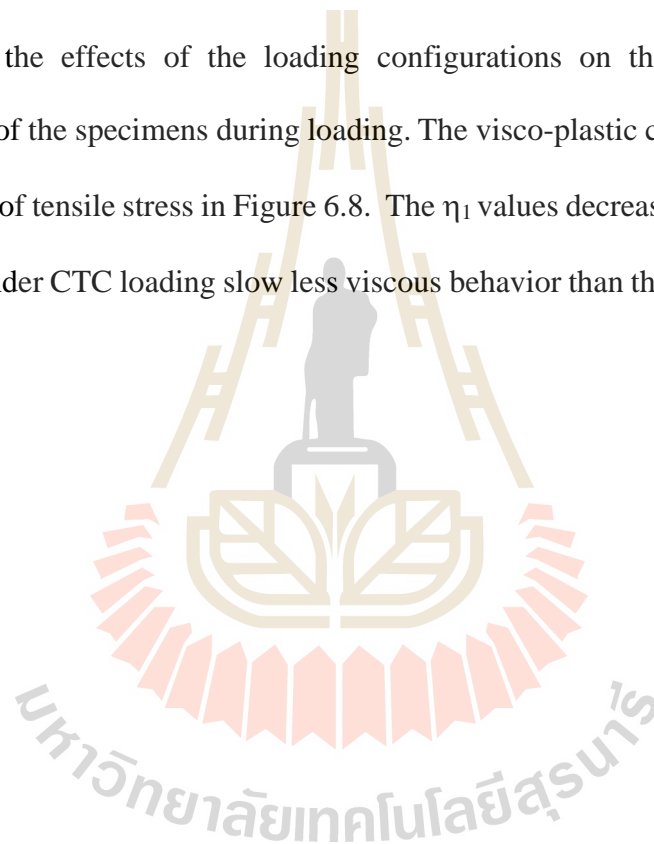
$$\varepsilon_x = \sigma_x / E \quad (6.2)$$

where E is the tensile elastic modulus of the salt. Using the Laplace transformation a linear visco-elastic relation can be derived from the above equation by using time operator of the Burgers model, and hence the tensile strain can be presented as a function of time (Richard, 1993):

$$\varepsilon_x(t) = \sigma_x [(t / \eta_1) + (1 / E_1) + (1 / E_2) (1 - \exp(-E_2 t / \eta_2))] \quad (6.3)$$

where σ_x is the applied constant tensile stresses (MPa), t is the testing time (day), E_1 is the tensile spring constant (GPa), E_2 is the spring constant in visco-elastic phase (GPa), η_1 is the viscosity coefficient in steady-state phase (GPa·Day), and η_2 is the viscosity coefficient in transient phase (GPa·Day).

Regression analyses on the strain-time curves for cyclic loading tests (Figures 6.6 and 6.7) based on Equation. (6.3) using the SPSS statistical software (Wendai, 2000) can determine the Burgers parameters for each specimen. Table 6.2 summarizes the calibration results. Relatively high variations of the calibrated Burgers parameters are observed. This may be explained by the complex mechanical responses of inclusions in the salt specimens. The visco-plastic coefficients (η_1) are used as an indicator of the effects of the loading configurations on the creep under cyclic deformation of the specimens during loading. The visco-plastic coefficients are plotted as a function of tensile stress in Figure 6.8. The η_1 values decrease as σ_t increases. The specimens under CTC loading show less viscous behavior than those under TC loading.



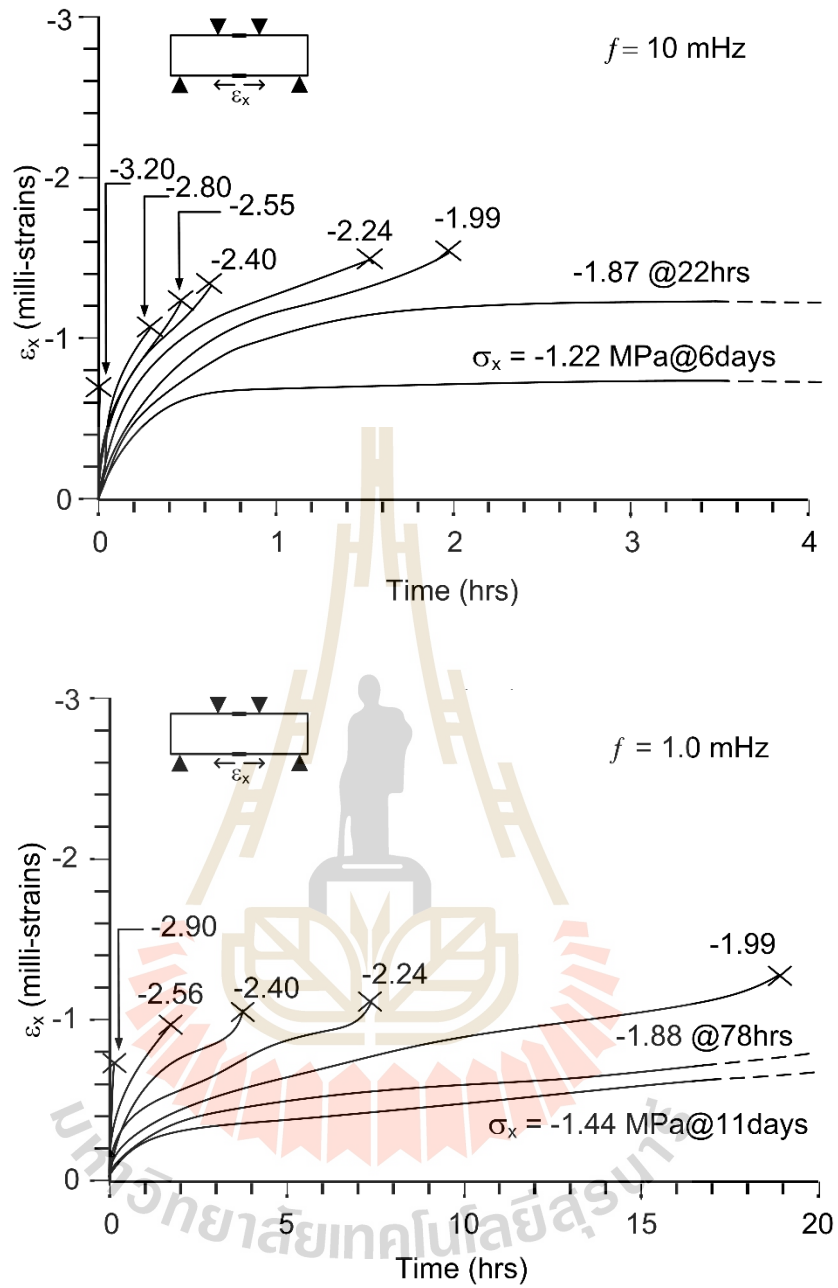


Figure 6.6 Tensile strains (ϵ_x) as a function of time for TC loading tests (Plangklang, 2017).

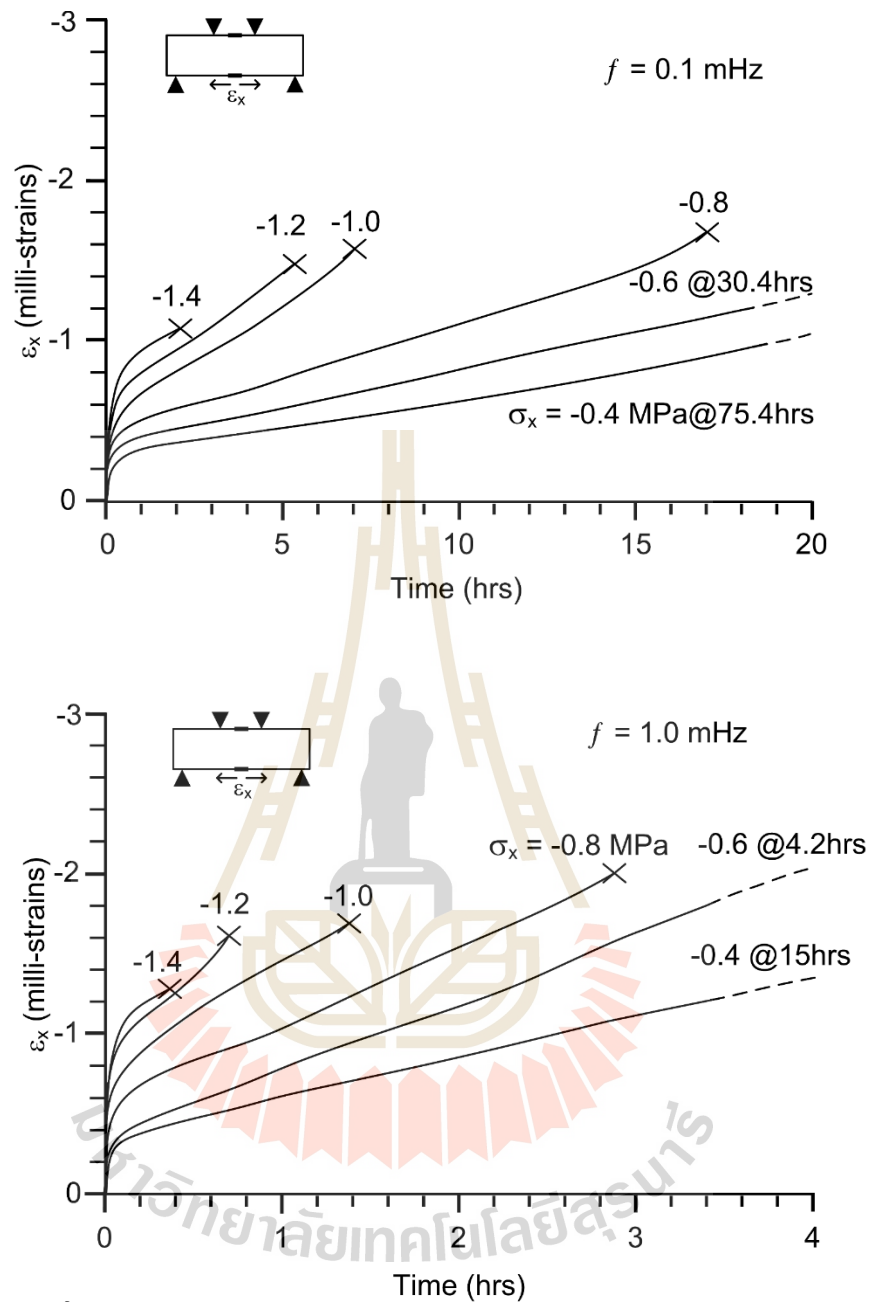


Figure 6.7 Tensile strains (ϵ_x) as a function of time for CTC loading tests.

Table 6.2 Burger parameters under TC (Plangklang, 2017) and CTC tests.

Loading configurations	σ_x (MPa)	Burger parameters				
		E_1 (GPa)	E_2 (GPa)	η_1 (GPa·Day)	η_2 (GPa·Day)	R^2
TC (10 mHz)	-2.80	6.52	4.01	0.07	0.08	0.91
	-2.55	6.41	3.89	0.07	0.06	0.88
	-2.40	6.45	3.78	0.12	0.06	0.90
	-2.24	5.22	2.71	0.21	0.06	0.95
	-1.99	5.13	2.55	0.33	0.04	0.91
	-1.87	5.02	2.41	0.39	0.04	0.84
	-1.22	4.33	2.23	0.73	0.03	0.93
TC (1 mHz)	-2.56	6.61	3.12	0.43	0.19	0.90
	-2.40	6.50	2.45	0.86	0.16	0.91
	-2.24	6.10	2.34	1.00	0.13	0.90
	-1.99	6.08	2.31	2.07	0.12	0.92
	-1.88	6.13	2.20	3.26	0.09	0.93
	-1.40	6.00	2.11	3.65	0.09	0.90
CTC (1 mHz)	-1.40	1.99	1.85	0.04	0.15	0.97
	-1.20	1.95	2.00	0.04	0.14	0.76
	-1.00	1.90	3.90	0.05	0.13	0.84
	-0.80	1.88	8.88	0.06	0.11	0.98
	-0.60	1.85	10.00	0.07	0.08	0.99
	-0.40	1.65	11.91	0.08	0.07	0.99
CTC (0.1 mHz)	-1.40	2.12	2.50	0.22	1.96	0.96
	-1.20	2.11	2.90	0.24	1.81	0.99
	-1.00	2.09	3.02	0.29	1.40	0.98
	-0.80	2.00	3.90	0.42	0.99	0.98
	-0.60	1.89	4.81	0.44	0.92	0.98
	-0.40	1.67	5.00	0.50	0.59	0.99

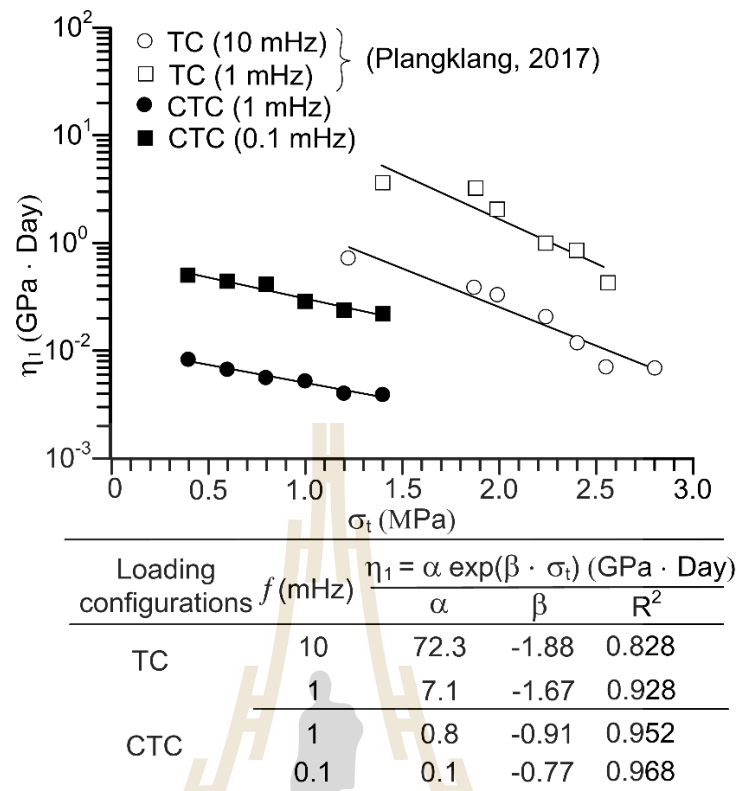


Figure 6.8 Visco-plastic coefficients (η_1) as a function of tensile stress for TC (Plangklang, 2017) and CTC tests.

CHAPTER VII

STRAIN ENERGY DENSITY CRITERION

7.1 Introduction

Strain energy density principle is applied to describe the effect of loading cycles and frequency on the fatigue tensile strengths of the rock salt specimens in the laboratory. This chapter describes the method of calculation and results. The results are also compared with those of Plangkang (2017) who performed testing on the same salt using different loading paths.

7.2 Strain energy density criterion

The strain energy density principle is applied here to consider both salt tensile stress and deformation at failure under different frequencies and amplitudes. The distortional, W_d and mean, W_m strain energy densities can be calculated from the maximum tensile stresses and strains for each salt specimen using the following relations (Jaeger et al., 2007):

$$W_d = (1/2) \cdot (s_x e_x + s_y e_y + s_z e_z) \quad (7.1)$$

$$W_m = (3/2) \cdot s \cdot e \quad (7.2)$$

where s and e are the mean stress and strain. The s_x , s_y and s_z are the stress deviations in major, intermediate and minor axes, and e_x , e_y and e_z are the strain deviations in major, intermediate and minor axes.

Assuming that the stress and strain obtained at the crack initiation point is in uniaxial stress condition; $\sigma_x \neq 0$, $\sigma_y = 0$, $\sigma_z = 0$, $\varepsilon_x \neq 0$, $\varepsilon_y \neq 0$ and $\varepsilon_z = 0$. The stress and strain deviations can be written as:

$$s = \sigma_x/3 \quad (7.3)$$

$$e = (\varepsilon_x + \varepsilon_y)/3 \quad (7.4)$$

$$s_x = \sigma_x - s \quad s_y = -s \quad s_z = -s \quad (7.5)$$

$$e_x = \varepsilon_x - e \quad e_y = \varepsilon_y - e \quad e_z = -e \quad (7.6)$$

where σ_x and ε_x are the maximum tensile stress and strain, ε_y is the lateral strain which can be determined by:

$$\varepsilon_y = -v\varepsilon_x \quad (7.7)$$

where v is the Poisson's ratio (v) which is determined from the Brazilian tension test, by Sriapai et al. (2012) as 0.33. Table 7.1 gives the results of the strain energy density calculation for the compression-to-tension cyclic loading obtained here.

Figure 7.1 shows a linear trend of the test data in the $W_d - W_m$ relation which can be represented by:

$$W_d = \eta \cdot W_m \quad (\text{kPa}) \quad (7.8)$$

where η is empirical constants ($\eta = 3.48 \text{ kPa}$) in this diagram the strain energy density relation obtained here are also compared with those of Plangklang (2017). The results show that they are on the same trend. The energy required to induce tensile failure for the CTC testing are lower than those of the monotonic loading (loading rates) and of the tension cyclic loading without reversing to compression (TC loading). The energy required to fail the specimens is lower for the lower loading frequencies. This also raises an issue that determining the stability of storage opening in rock salt by using the monotonic loading such as suggesting by the ASTM standard may not be conservative.

Table 7.1 Strain energy densities of cyclic loading.

f (mHz)	σ_x (MPa)	ϵ_x (milli-strains)		ϵ_y (milli-strains)		s (MPa)	e (milli-strains)		W_d (kPa)	W_m (kPa)
		Tension	Com- pression	Tension	Com- pression		Tension	Com- pression		
1	-1.40	-1.27	0.63	-0.21	0.42	± 0.47	-0.28	0.14	1.03	0.30
	-1.20	-1.62	0.68	-0.22	0.53	± 0.40	-0.36	0.15	1.07	0.31
	-1.00	-1.68	0.65	-0.21	0.55	± 0.33	-0.38	0.14	0.90	0.26
	-0.80	-1.99	0.83	-0.27	0.66	± 0.27	-0.44	0.19	0.88	0.25
	-0.60	-2.14	0.81	-0.27	0.71	± 0.20	-0.48	0.18	0.69	0.20
	-0.40	-3.33	1.47	-0.49	1.10	± 0.13	-0.74	0.33	0.75	0.21
0.1	-1.40	-1.08	0.49	-0.16	0.36	± 0.47	-0.24	0.11	0.85	0.24
	-1.20	-1.47	0.68	-0.22	0.49	± 0.40	-0.33	0.15	1.00	0.29
	-1.00	-1.57	0.50	-0.17	0.52	± 0.33	-0.35	0.11	0.80	0.23
	-0.80	-1.67	0.70	-0.23	0.55	± 0.27	-0.37	0.16	0.73	0.21
	-0.60	-1.85	0.81	-0.27	0.61	± 0.20	-0.41	0.18	0.62	0.18
	-0.40	-3.04	1.30	-0.43	1.00	± 0.13	-0.68	0.29	0.67	0.19

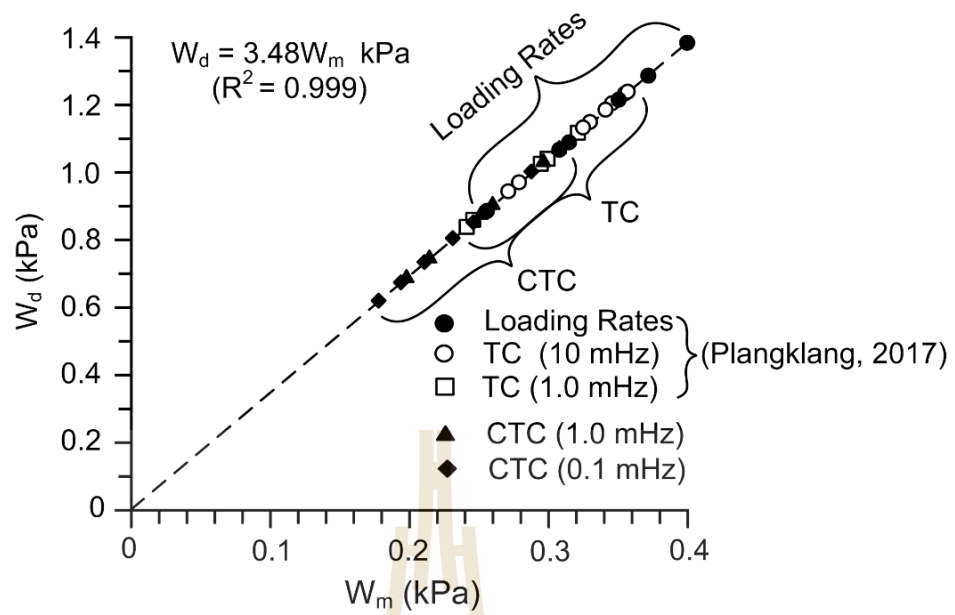
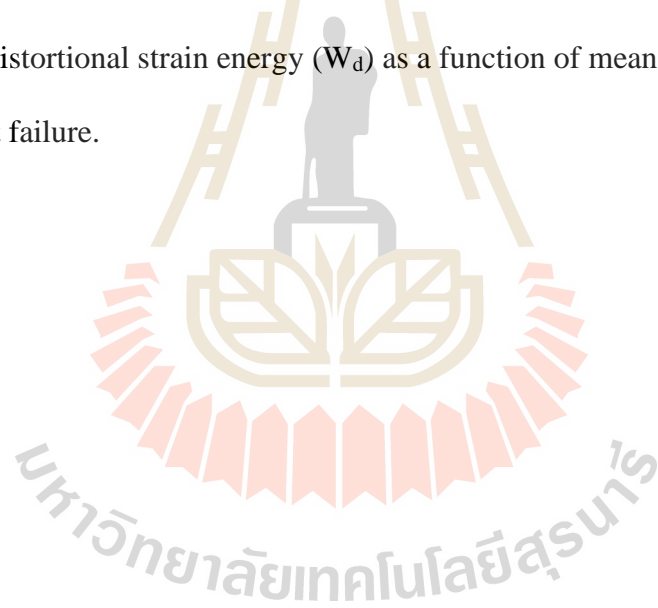


Figure 7.1 Distortional strain energy (W_d) as a function of mean strain energy (W_m) at failure.



CHAPTER VIII

DISCUSSIONS, CONCLUSIONS AND RECOMMENDATIONS FOR FUTURE STUDIES

8.1 Discussions

This section discusses the key issues relevant to the reliability of the test schemes and the adequacies of the test results. Comparisons of the results and findings from this study with those obtained elsewhere under similar test conditions have also been made.

The effect of cyclic loading on rock salt under uniaxial and triaxial compression tests has been investigated to determine the fatigue lives of the storage cavern wall in salt mass (Fan et al., 2016, 2017; Song et al., 2013; Yasong et al., 2016). Some researchers have studied the effect of tensile cyclic loading on the mechanical behavior of several rock types, such as Erarslan and Williams (2012) studied on Brisbane tuff, Voznesenskii et al. (2016) on gypsum, Cardani and Meda (2004) on marble and Wang et al. (2016) on rock salt. The loading cycles can reduce the fatigue strength and elastic modulus, depending on the loading amplitudes (Ren et al., 2013; Guo et al., 2012), loading frequency (Momeni et al., 2015) and maximum applied loads for each cycle (Song et al., 2013; Wang et al., 2016).

The four-point bending test is more preferable than the others because it is the simplest method whose stress configurations are similar to those in the cavern roof.

The post-test specimens obtained from the four-point bending test show that the tension crack occurs at the center of specimen for all specimen beams. This suggests that the test results are valid. Plangklang (2017) performed four-point bending under tension cyclic loading tests without reversing to compression (TC). The loading frequencies range from 1 to 10 mHz. The induced maximum tensile stresses range from 1.21 to 3.20 MPa. The results indicate that the permanent strains increase and accumulate from each cycle until the specimen fails. The number of loading cycle increases with decreasing the stress amplitudes. Elastic modulus of rock salt derived from each cyclic loading cycle decrease as the number of cycles increase.

Similar behaviour also observed with the compression-to-tension cyclic loading (CTC) performed here. The results indicate that the maximum number of loading cycles increases with decreasing stress amplitudes. The effect of loading frequencies tends to be relatively small. The lower frequencies tend to induce lower fatigue stress.

The results obtained here are compared with the tension cyclic loading (TC) that was obtained by Plangklang (2017). It is clear the loading paths can affect the tensile fatigue strengths of rock salt. The tensile fatigue strengths under CTC loading paths are about half of those under TC loading path (Figure 6.2). This is probable because under the same stress amplitude, rock salt under CTC loading can accumulate the tensile strain for each cycle more quickly than those under TC loading. Here the loading amplitudes for tension and compression are equal for each specimen. It postulates that the reductions of the fatigue strength would be enhanced if the compression loading amplitude is higher than the tensile loading amplitude. This phenomenon would likely occur under actual in-situ condition (in the roof of salt storage cavern). The small effect

of the loading frequencies observed here under tensions is similar to those observed by Fuenkajorn and Phueakphum (2010) under compression on the same rock salt.

8.2 Conclusions

All objectives and requirements of this study have been met. The results of the laboratory testing and analyses can be concluded as follows:

1) The tensile stress-strain curves can be measured during cyclic loading, as shown in Figure 5.1. The number of loading cycles increases with decreasing stress amplitudes and frequencies. The accumulated strains at failure increase as the amplitudes and loading frequencies are decreased. The elastic modulus decreases with increasing stresses amplitudes and frequencies.

2) The fatigue tensile stresses (σ_x) as a function of loading cycles, e.g. S-N curves are plotted in Figure 5.2. The effect of loading frequencies tends to be relatively small. The lower frequencies tend to induce lower fatigue stress.

3) The normalized tensile elastic modulus (E/E_0) is plotted as a function of a number of loading cycles. The normalized elastic modulus rapidly decreases with increasing loading cycles in Figure 5.3. The specimens tested under low loading frequencies show the normalized elastic modulus lower than those under higher frequencies.

4) The induced-fractures are clean and well mated. More inter-granular fracturing is found in specimens tested under low loading frequency than under high loading frequency. As a result, fractures induced under high loading frequency appear to be smoother than those under low loading frequency.

5) The tensile strain-time curves compiled from loci of the loading cycles by plotting the maximum point of each cycles. The curves show the transient, steady-state and tertiary creep phases which are similar to those obtained from static compression creep testing. The cyclic loading test results indicate that the maximum number of loading cycles increases with decreasing the stress amplitudes.

6) Strain energy density principle is applied to describe the effect of loading cycles on the fatigue tensile strengths of the salt specimens primarily because it considers both stress and strain at failure. The energy required to induce tensile failure for the low stress frequency is lower than those obtained from the high stress frequency. The energy for CTC testing is also lower than those obtained by Plangklang (2017) on the monotonic testing and on the TC testing.

8.3 Recommendations for future studies

1) More laboratory tests should be performed by emphasizing on the effects of stress levels and temperatures. This would be similar to that occur during product injection and retrieval in storage cavern in rock salt.

2) Numerical modelling should be performed to calculate tensile stresses in cavern roof by compared and confirm the accuracy with the test results in the laboratory.

3) The test specimens here are relatively small. Testing on larger specimens is desirable in order to will be closer to the in-situ conditions and confirm the research findings.

4) Effects of inclusions on the tensile fatigue stress of rock salt have not been studied here. Anhydrite and some clay mineral are sometimes found in the Maha Sarakham salt. The effects of such inclusions should be assessed on the tensile fatigue of the salt.



REFERENCES

- ASTM C293-02. Standard test method for flexural strength of concrete (Using simple beam with center-point loading). **Annual Book of ASTM Standards**, Vol. 04.08. West Conshohocken: American Society for Testing and Materials.
- ASTM D6272-10. Standard test method for flexural properties of unreinforced and reinforced plastics and electrical insulating materials by four-point bending. **Annual Book of ASTM Standards** (Vol. 04.08). Philadelphia: American Society for Testing and Materials.
- Cardani, G. and Meda, A. (2004). Marble behaviour under monotonic and cyclic loading in tension. **Construction and Building Materials**. 18(6): 419–424.
- Chan, G.C., Thompson, P.A., Allen, R.A., and Loscutoff, W.V. (1980). Underground compressed air energy storage for electric utilities, **Subsurface**. 2: 579-585.
- Chobsranoi, M. and Fuenkajorn, K. (2016). Maximum unsupported span and standup time of potash mine roof as affected by carnallite contents. In **the Ninth Asian Rock Mechanics Symposium**. 18-20 October 2016, Bali, Indonesia.
- Crotogino, F., Mohmeyer, W. U., and Scharf, R. (2001). **Huntorf CAES: More Than 20 Years of Successful Operation**. Spring 2001 Meeting, Orlando, Florida, USA.
- DeLong, M.M., Nelson, C.R., and Petersen, D.L. (1989). Subsurface cavern system requirements for compressed air energy storage and associated uses. In Nilsen

- and Olsen (eds.). **Storage of Gases in Rock Caverns** (ISBN 906191 896 0). Balkema, Rotterdam. pp. 33-36.
- Dusseault, M.B. and Fordham, C.J. (1993). Time-dependent behavior of rocks. **Comprehensive Rock Engineering Principles, Practice and Project: Rock Testing and Site Characterization**. London, Pergamon. 3: 119-149.
- EPRI. (1986). **Dynamic Operating Benefits of Energy Storage**. EPRI Report No.AP-4875, Palo Alto, CA, Electric Power Research Institute.
- EPRI. (1990a). **Compressed Air Storage for Electric Power Generation**. EPRI Report No.GS-6784, Palo Alto, CA, Electric Power Research Institute.
- EPRI. (1990b). **Compressed-Air Energy Storage using Hard-Rock Geology**. Palo Alto, CA, Electric Power Research Institute.
- EPRI. (1990c). **Rock Concern Linings for Compressed-Air Energy Storage**. Palo Alto, CA, Electric Power Research Institute.
- EPRI. (1992a). **Alabama Electric Cooperative (AEC) Builds First U.S. Compressed Air Energy Storage (CAES) Plant Using EPRI-Developed Low-Pressure Expander**. EPRI Report No.IN-101511, Palo Alto, CA, Electric Power Research Institute.
- EPRI. (1992b). **CAES goes on-line [Video recording]**. Palo Alto, CA, Electric Power Research Institute.
- EPRI. (1992c). **EPRI-Developed Acquisition System Monitors Compressed-Air Energy Storage (CASE) Plant On-line Performance**. EPRI Report No.IN-101510, Palo Alto, CA, Electric Power Research Institute.
- EPRI. (1994a). **Compressed Air Handbook**. EPRI Report No. CR-104546, Palo Alto, CA, Electric Power Research Institute.

- EPRI. (1994b). **Comprehensive Analyses of Compressed–Air Cycles; CAES, CAES-ES, CRCAES/CRCASH-ES, and MRCAES/MRCASH-ES.** EPRI Report No.TR-103521, Palo Alto, CA, Electric Power Research Institute.
- EPRI. (1994c) **Development of Turbomachinery Trains for the CASHING, NGCASH, and IGCASH Cycle Applications.** EPRI Report No.TR-103348, Palo Alto, CA, Electric Power Research Institute.
- EPRI. (1994e). **Standard Compressed-Air Energy Storage Plant: Design and Cost.** Research Project No. TR-103209, Palo Alto, CA, Electric Power Research Institute.
- EPRI. (1997). **Energy Storage in a Restructured Electric Utility Industry: Report on EPRI Think Tanks I and II.** EPRI Report No.TR-108894, Palo Alto, CA, Electric Power Research Institute.
- EPRI. (1999). **Conceptual Engineering and Cost Estimate for 100-MW and 20MW Nominal Capacity CASH Plants.** EPRI Report No.TR-113360, Palo Alto, CA, Electric Power Research Institute.
- Erarslan, N. and Williams, D.J. (2012). Investigating the effect of cyclic loading on the indirect tensile strength of rocks. **Rock Mechanics and Rock Engineering.** 45(3): 327-340.
- Fan, J., Chen, J., Jiang, D., Chemenda, A., Chen J., and Ambre, J. (2017). Discontinuous cyclic loading tests of salt with acoustic emission monitoring. **International Journal of Fatigue.** 94: 140-144.
- Fan, J., Cnen, J., Jiang, D., Ren, S., and Wu, J. (2016). Fatigue properties of rock salt subjected to interval cyclic pressure. **International Journal of Fatigue.** 90: 109-115.

- Forster, I. (1967). Stability Investigations Applied to Mining of Evaporates, **Ph.D. Thesis**. University of Newcastle upon Tyne.
- Fuenkajorn, K. and Daemen, J.J.K. (1988). Boreholes closure in salt. **Technical Report Prepared for The U.S. Nuclear Regulatory Commission**. Report No. NUREG/CR-5243 RW. University of Arizona.
- Fuenkajorn, K. and Daemen, J.J.K. (1992a). Borehole sealing, compressed-air energy storage. In **Proceedings of the Second International Conference. Electric Power Research Institute** (pp. 5.1-5.21), July 7-9, San Francisco, CA.
- Fuenkajorn, K. and Phueakphum, D. (2010). Effects of cyclic loading on mechanical properties of Maha Sarakham salt. **Engineering Geology**. 112(1-4): 43-52.
- Fuenkajorn, K. and Serata, S. (1992). Geohydrological integrity of CAES in rock salt. In **Proceedings of the second International Conference on Compressed Air Energy Storage, Electric Power Research Institute** (pp. 4.1-4.21). San Francisco.
- Gehle, R.M. and Thoms, R.L. (1986). **Tests of U.S. Rock Salt for Long-Term Stability of CAES Reservoirs**. Richland, Wash: Pacific Northwest Laboratory.
- Gere, J.M. (2004). Stresses in Beams (Basic Topics). **Mechanics of Materials**. Bill Stenquist. pp. 300-314.
- Gnirk, P.F. and Johnson, R.E. (1964). The deformational behavior of a circular mine shaft situated in a viscoelastic medium under hydrostatic stress. In **Proceedings of the Sixth U.S. Symposium on Rock Mechanics** (pp. 233-259). University of Missouri, Rolla.

- Guo, Y., Yang, C., and Mao, H. (2012). Mechanical properties of Jintan mine rock salt under complex stress paths. **International Journal of Rock Mechanics and Mining Sciences**. 56: 54-61.
- Haimson, B.C. (1978). Effect of cyclic loading on rock. **Dynamic Geotechnical Testing**. ASTM STP 654. pp. 228-245.
- Handin, J., Russell, J.E., and Carter, N.L. (1984). Transient creep of repository rocks. **Final Report: Mechanistic Creep Laws for Rock Salts**, Texas A & M research Foundation, Office of Nuclear Waste Isolation, Battelle Memorial Institute, Report, BMI/ONWI-550.
- Hardy, H.R. and Sun, X. (1986). A nonlinear rheological model for time-dependent behavior of geologic materials. In **Proceedings of Twenty-Seventh U.S. Symposium on Rock Mechanics** (pp. 205-212). June 23-25, University of Alabama, Tuscaloosa, Howard L, Hartman ed., Ch.2.
- Jaeger, J.C., Cook, N.G.W., and Zimmerman, R.W. (2007). **Fundamentals of Rock Mechanics Fourth Edition**, fourth edition, Blackwell publishing, Oxford.
- Jeremic, M.L. (1994). **Rock Mechanics in Salt Mining**. Rotherdam: A. A. Balkema. pp. 530.
- Katz, D.L. and Lady, E.R. (1976). **Compressed Air Storage**, Ann Arbor, Michigan: Ulrich's Book.
- Knowles, M.K., Borns, D., Fredrich, J., Holcomb, D., Price, R., and Zeuch, D. (1998). Testing the disturbed zone around a rigid inclusion in salt. In **Proceedings of the Fourth Conference on the Mechanical Behavior of Salt** (pp. 175-188). Clausthal, Germany, Trans Tech Publications.

- Kumar, A. (1968). The effect of stress rate and temperature on the strength of basalt and granite. **Geophysics**. 33(3): 501-510.
- Langer, M. (1984). The rheological behaviour of rock salt, mechanical behavior of salt. In **Proceedings of the First Conference on the Mechanical Behavior of Salt** (pp. 201-240). November 9-11, 1981, The Pennsylvania State University, Trans Tech Publications, ClausthalZellerfeld, Federal Republic of Germany.
- Liang, W.G., Zhao, Y.S., Xu, S.G., and Dusseault, M.B. (2010). Effect of strain rate on the mechanical properties of salt rock. **International Journal of Rock Mechanics and Mining Sciences**. 48: 161-167.
- Liu, L.F., Pei, J.L., Ma, K., Zhou, H., and Hou, Z. (2010). Underground Storage of CO₂ and Energy. In **Proceedings of the Sino-German Conference** (pp. 105-112). Beijing, China.
- Ma, L.J., Liu, X.Y., Wang, M.Y., Xu, H.F., Hua, R.P., Fan, P.X., Jiang, S.R., Wang, G.A., and Yi, Q.K. (2013). Experimental investigation of the mechanical properties of rock salt under triaxial cyclic loading. **International Journal of Rock Mechanics and Mining Sciences**. 62: 34-41.
- Momeni, A., Karakus, M., Khanlari, G.R., and Heidari, M. (2015). Effects of cyclic loading on the mechanical properties of a granite. **International Journal of Rock Mechanics and Mining Sciences**. 77:89–96.
- Obert, L. and Duvall, W.I. (1967). **Rock Mechanics and the Design of Structures in Rock**. John Wiley and Sons. pp. 649.

- Passaris, E.K.S. (1982). Fatigue characteristics of rock salt with reference to underground storage cavern. In **Proceedings International Society for Rock Mechanics Symposium** (pp. 983-989). Aachen.
- Plangklang, J. (2017). Time-dependent tensile strength and deformability of rock salt using four-point bending test. **Master Thesis**. Suranaree University of Technology.
- Ren, S., Bai, Y.M., Zhang, J.P., Jiang, D.Y., and Yang, C.H. (2013). Experimental investigation of the fatigue properties of salt rock. **International Journal of Rock Mechanics and Mining Sciences**. 64(1): 68-72.
- Richard, J. (1993). Plasticity and creep. Theory, example, and problems, english edition editor, **Rochester Institute of Technology**, Rochester, New York.
- Sen, G.C. (1961). An investigation into the stability of room and pillar workings in rock salt. **Ph.D. Thesis**. University of Newcastle upon Tyne.
- Senseny, P.E. (1984). Specimen size and history effects on creep of salt. In **Proceedings of the First Conference on the Mechanics Behavior of Salt** (pp. 369-379). Clausthal-Zellerfeld: Trans Tech Publications.
- Serata, S., Mehta, B., and Hiremath, M. (1989). Geomechanical stability analysis for CAES cavern operation, In Nilsen and Olsen (eds). **Storage of Gases in Rock Caverns** (pp. 129-135). Balkema, Rotterdam.
- Snyder, V.W. (1983). Analysis of beam building using fully grouted roof bolts. In **Proceedings of the International Symposium on Rock Bolting** (pp. 187-194). Abisko, Sweden.

- Song, R., Yue-ming, B., Jing-Peng, Z., De-yi, J., and Chum-he, Y. (2013). Experimental investigation of the fatigue properties of salt rock. **International Journal of Rock Mechanics and Mining Sciences**. 64: 68-72.
- Sriapai, T., Walsri, C., and Fuenkajorn, K. (2012). Effect of temperature on compressive and tensile strength of salt. **ScienceAsia**. 38: 166-174.
- Stimpson, B. and Ahmed, M. (1992). Failure of a linear voussoir arch: a laboratory and numerical study. **Canadian Geotechnical Journal**. 29: 188-194.
- Thirumalai, K. and Demou, S.G. (1974). Thermal expansion behavior of intact and thermally fractured mine rocks. **International Journal of Rock Mechanics and Mining Sciences**. 17: 60-71.
- Thoms, R.L. and Martinez, J. D. (1978). Preliminary long-term stability criteria for compressed air energy storage caverns in salt domes. **Prepared for Battelle Northwest Laboratories, Richland, Washington, Special Agreement B-54804-A-L, Prime Contact EY-76-C-06-1830, 84 p.** Institute for Environmental Studies, Louisiana Studies, Louisiana University, Baton Rouge, LA.
- Thoms, R. L., Nathany, M., and Gehle, R. (1980). Low-frequency cyclic loading effect in rock salt. In **Proceedings of the International Symposium on Subsurface Space (Rockstore 80)** (pp. 755-761). Stockholm.
- Voznesenskii, A.S., Krasilov, M.N., Kutkin, Y.O., Tavostin, M.N., and Osipov, Y.V. (2017). Features of interrelations between acoustic quality factor and strength of rock salt during fatigue cyclic loadings. **International Journal of Fatigue**. 97: 70-78.

- Voznesenskii, A.S., Kutkin, Y.O., Krasilov, M.N., and Komissarov, A.A. (2016). The influence of the stress state type and scale factor on the relationship between the acoustic quality factor and the residual strength of gypsum rocks in fatigue tests. **International Journal of Fatigue.** 84:53–58.
- Wang, W., Wang, M., and Liu, X. (2016). Study on mechanical features of brazilian splitting fatigue tests of salt rock. **Advances in Civil Engineering.** pp. 1-10.
- Warren, J. (1999). **Evaporites: Their evolution and economics.** Philadelphia: Blackwell Science. pp. 235-239.
- Wendai, L. (2000). Regression analysis, linear regression and probity regression in 13 chapters. **SPSS for Windows: statistical analysis.** Publishing House of Electronics Industry. Beijing.
- Wisetsaen, S., Walsri, C., and Fuenkajorn, K. (2015). Effects of loading rate and temperature on tensile strength and deformation of rock salt. **International Journal of Rock Mechanics and Mining Sciences.** 73: 10-14.
- Wittke, W., Pierau, B., and Schetelig, K. (1980). Planning of a compressed-air pumped-storage scheme at Vianden/Luxemboueg. In **Proceedings of the International Symposium on Subsurface Space, Rockstore 80** (2: 367-376). Stockholm.
- Xiao, J.Q., Ding, D.X., Jiang, F.L., and Xu, G. (2010). Fatigue damage variable and evolution of rock subjected to cyclic loading. **International Journal of Rock Mechanics and Mining Sciences.** 47: 461–468.
- Yokoyama, T.A. (1988). A microcomputer-aided four-point test system for determining uniaxial stress-strain curves. **Journal of Testing and Evaluation.** 16: 198-204.

Yasong, W., Linjian, M., Pengxian, F., and Yan, C. (2016). A fatigue damage model for rock salt considering the effects of loading frequency and amplitude.

International Journal of Mining Science and Technology. 26:955-958.

Zhang, X. and Wong, L.N.Y. (2014). Choosing a proper loading rate for bonded-particle model of intact rock. **International Journal of Fracture rock.** 189(2): 163-

179.





APPENDIX A

PUBLICATION

Publication

Kaewpuang, T., Plangklang, J., Khamrat, S., and Fuenkajorn, K. (2018). Effects of cyclic loading on tensile strength of rock salt. In **12th South East ASEAN Technical University Consortium Symposium (SEATUC2018)**. March 12-13, University Gadjah Mada, Yogyakarta, Indonesia.



BIOGRAPHY

Mr.Thanapon Keawpuang was born on September 30, 1994 in Ubon Ratchathani, Thailand. He received her Bachelor's Degree in Engineering (Geological Engineering) from Suranaree University of Technology in 2016. For her post-graduate, she continued to study with a Master's degree in the Geotechnology Program, Institute of Engineering, Suranaree university of Technology. During graduation, 2017-2018, he was a part time worker in position of research assistant at the Geomechanics Research Unit, Institute of Engineering, Suranaree University of Technology.

